

1 Evaluation of potential sources of a priori ozone profiles for 2 TEMPO tropospheric ozone retrievals

3 Matthew S. Johnson¹, Xiong Liu², Peter Zoogman^{2,*}, John Sullivan³, Michael J. Newchurch⁴, Shi
4 Kuang⁵, Thierry Leblanc⁶, Thomas McGee³

5 ¹Earth Science Division, NASA Ames Research Center, Moffett Field, CA, USA.

6 ²Harvard-Smithsonian Center for Astrophysics, Cambridge, MA, USA.

7 ³Atmospheric Chemistry and Dynamics Laboratory, NASA Goddard Space Flight Center, Greenbelt, Maryland, USA.

8 ⁴Atmospheric Science Department, University of Alabama in Huntsville, Huntsville, AL, USA.

9 ⁵Earth System Science Center, University of Alabama in Huntsville, Huntsville, AL, USA.

10 ⁶Table Mountain Facility, California Institute of Technology, Wrightwood, CA, USA.

11 *also at Minerva Schools at KGI, San Francisco, CA, USA.

12 *Correspondence to:* Matthew S. Johnson (matthew.s.johnson@nasa.gov)

13 **Abstract.** Potential sources of a priori ozone (O₃) profiles for use in Tropospheric Emissions: Monitoring of Pollution
14 (TEMPO) satellite tropospheric O₃ retrievals are evaluated with observations from multiple Tropospheric Ozone Lidar
15 Network (TOLNet) systems in North America. An O₃ profile climatology (tropopause-based O₃ climatology (TB-
16 Clim), currently proposed for use in the TEMPO O₃ retrieval algorithm) derived from ozonesonde observations and
17 O₃ profiles from three separate models (operational Goddard Earth Observing System (GEOS-5) Forward Processing
18 (FP) product, reanalysis product from Modern-Era Retrospective analysis for Research and Applications version 2
19 (MERRA2), and the GEOS-Chem chemical transport model (CTM)) were: 1) evaluated with TOLNet measurements
20 on various temporal scales (seasonally, daily, hourly) and 2) implemented as a priori information in theoretical
21 TEMPO tropospheric O₃ retrievals in order to determine how each a priori impacts the accuracy of retrieved
22 tropospheric (0-10 km) and lowermost tropospheric (LMT, 0-2 km) O₃ columns. We found that all sources of a priori
23 O₃ profiles evaluated in this study generally reproduced the vertical structure of summer-averaged observations.
24 However, larger differences between the a priori profiles and lidar observations were observed when evaluating inter-
25 daily and diurnal variability of tropospheric O₃. The TB-Clim O₃ profile climatology was unable to replicate observed
26 inter-daily and diurnal variability of O₃ while model products, in particular GEOS-Chem simulations, displayed more
27 skill in reproducing these features. Due to the ability of models, primarily the CTM used in this study, on average to
28 capture the inter-daily and diurnal variability of tropospheric and LMT O₃ columns, using a priori profiles from CTM
29 simulations resulted in TEMPO retrievals with the best statistical comparison with lidar observations. Furthermore,
30 important from an air quality perspective, when high LMT O₃ values were observed, using CTM a priori profiles
31 resulted in TEMPO LMT O₃ retrievals with the least bias. The application of time-specific (non-climatological)
32 hourly/daily model predictions as the a priori profile in TEMPO O₃ retrievals will be best suited when applying this
33 data to study air quality or event-based processes as the standard retrieval algorithm will still need to use a climatology
34 product. Follow-on studies to this work are currently being conducted to investigate the application of different CTM-
35 predicted O₃ climatology products in the standard TEMPO retrieval algorithm. Finally, similar methods to those used
36 in this study can be easily applied by TEMPO data users to recalculate tropospheric O₃ profiles provided from the
37 standard retrieval using a different source of a priori.

38 **1 Introduction**

39 Ozone (O₃) is an important atmospheric constituent for air quality as concentrations above natural levels can have
40 detrimental health impacts (US EPA, 2006) and the United States (US) Environmental Protection Agency (EPA)
41 enforces surface-level mixing ratios under the National Ambient Air Quality Standards (NAAQS). In 2015, the
42 NAAQS for O₃ was reduced from prior levels of 75 parts per billion (ppb) to 70 ppb, requiring that 3-year averages
43 of the annual fourth-highest daily maximum 8-hour mean mixing ratio must be ≤ 70 ppb (US EPA, 2015).
44 Tropospheric and surface-level O₃ mixing ratios are controlled by a complex system of photo-chemical reactions
45 involving numerous trace gas species (e.g., carbon monoxide (CO), methane, volatile organic compounds, and
46 nitrogen oxides (NO_x = nitric oxide and nitrogen dioxide (NO + NO₂)) emitted from anthropogenic and natural sources
47 (Atkinson, 1990; Lelieveld and Dentener, 2000). Furthermore, a portion of tropospheric O₃ is also contributed from
48 the downward transport from the stratosphere, commonly referred to as stratosphere-to-troposphere exchange (STE)
49 (e.g., Stohl et al., 2003; Lin et al., 2015; Langford et al., 2017). Due to the complex chemistry and vertical/horizontal
50 transport processes controlling O₃ mixing ratios, and the continued reduction of NAAQS levels, it is increasingly
51 important to improve the ability to monitor/study tropospheric and surface-level O₃.

52 The monitoring of air quality in North America is typically conducted by using ground-based in situ
53 measurement networks. However, in recent years, observations of tropospheric O₃ and precursor gases (e.g., CO, NO₂,
54 formaldehyde (HCHO)) have been made from space-borne platforms which have led to the better understanding of
55 the tropospheric O₃ budget (Sauvage et al., 2007; Martin, 2008; Duncan et al., 2014). Total column (stratosphere +
56 troposphere) O₃ has been routinely measured by numerous space-based sensors since the launch of the Total Ozone
57 Mapping Spectrometer (TOMS) in 1978. Tropospheric column O₃ has been derived from total column retrievals using
58 strategies such as residual-based approaches which subtract the stratospheric column O₃ from total O₃ (Fishman et al.,
59 2008 and references therein). Tropospheric O₃ profiles have also been directly retrieved from hyperspectral Ultraviolet
60 (UV) (e.g., Liu et al., 2005, 2010) and Thermal Infrared (TIR) (e.g., Bowman et al., 2006) measurements. Currently,
61 sensors measuring tropospheric O₃, such as those using UV measurements from the Ozone Monitoring Instrument
62 (OMI) and TIR measurements from the Tropospheric Emission Spectrometer (TES) (Beer, 2006), are from low earth
63 orbit (LEO). While LEO provides global coverage, the observation of tropospheric O₃ is limited by coarse spatial
64 resolution, limited temporal frequency (once or twice per day), and inadequate sensitivity to lower tropospheric and
65 planetary boundary layer (PBL) O₃ (Fishman et al., 2008; Natraj et al., 2011). These limitations restrict the ability to
66 apply these space-borne observations in air quality policy and monitoring.

67 The Tropospheric Emissions: Monitoring of Pollution (TEMPO) instrument, which will be launched between
68 2019-2021 to geostationary orbit (GEO), is designed to address some of the limitations of current O₃ remote-sensing
69 instruments (Chance et al., 2013; Zoogman et al., 2017). TEMPO will provide critical measurements such as vertical
70 profiles of O₃, total column O₃, NO₂, sulfur dioxide, HCHO, glyoxal, and aerosol/cloud parameters over North
71 America. These data products will be provided at temporal resolutions as high as hourly and at a native spatial
72 resolution of $\sim 2.1 \times 4.4$ km² (at the center of the field of regard) except at the required spatial resolution of 8.4×4.4
73 km² for the O₃ profile product (four pixels combined to increase signal to noise ratios and reduce computational
74 resources). TEMPO's domain will encompass the region of North America from Mexico City to the Canadian oil

75 sands and from the Atlantic to the Pacific Ocean. TEMPO will have increased sensitivity to lower tropospheric O₃
76 compared to past/current satellite data by combining measurements from both UV (290-345 nm) and visible (VIS,
77 540-650 nm) wavelengths (Natraj et al., 2011; Chance et al., 2013; Zoogman et al., 2017). The operational TEMPO
78 O₃ product will provide vertical profiles and partial O₃ columns at ~24-30 layers from the surface to ~60 km above
79 ground level (agl). This product will also include total, stratospheric, tropospheric, and a 0-2 km above ground level
80 O₃ columns. TEMPO's high spatial and temporal resolution measurements, including the 0-2 km O₃ column, will
81 provide a wealth of information to be used in air quality monitoring and research.

82 Vertical O₃ profile retrievals from TEMPO will be based on the Smithsonian Astrophysical Observatory
83 (SAO) O₃ profile algorithm which was developed for use in the Global Ozone Monitoring Experiment (GOME) (Liu
84 et al., 2005), OMI (Liu et al., 2010), GOME-2 (Cai et al., 2012), and the Ozone Mapping and Profiler Suite (Bak et
85 al., 2017). Currently, the SAO O₃ retrieval algorithm for TEMPO has been proposed to apply the tropopause-based
86 O₃ climatology (TB-Clim) developed in Bak et al. (2013) as the a priori profiles (Zoogman et al., 2017), which was
87 demonstrated to improve OMI O₃ retrievals near the tropopause compared to calculations using the Labow-Logan-
88 McPeters (LLM) O₃ climatology (a priori used for OMI) (McPeters et al., 2007). During this work, we evaluate the
89 representativeness of the vertical O₃ profiles from TB-Clim. Additionally, we evaluate simulated time-specific (non-
90 climatological) O₃ profiles from an operational near-real-time (NRT) data assimilation model product (National
91 Aeronautics and Space Administration (NASA) Global Modeling and Assimilation Office (GMAO) Goddard Earth
92 Observing System (GEOS-5) Forward Processing (FP)), a reanalysis data product (NASA GMAO Modern-Era
93 Retrospective analysis for Research and Applications version 2 (MERRA2)), and a chemical transport model (CTM)
94 (GEOS-Chem). The climatology and model O₃ profiles were evaluated with ground-based lidar data from the
95 Tropospheric Ozone Lidar Network (TOLNet) at various locations of the US during the summer of 2014. This
96 evaluation focused on the performance of each product compared to summer-, daily-, and hourly-averaged lowermost
97 tropospheric (LMT, 0-2 km) and tropospheric (0-10 km) O₃ columns. Furthermore, based on past studies
98 demonstrating the importance of a priori profiles in trace gas satellite retrievals (Martin et al., 2002; Luo et al., 2007;
99 Kulawik et al., 2008; Zhang et al., 2010, Bak et al., 2013), we evaluated the effectiveness of using the TB-Clim and
100 model products as a priori in the TEMPO O₃ profile algorithm.

101 This paper is organized as follows. Section 2 describes the tropospheric lidar O₃ measurements, TB-Clim and
102 model products, theoretical TEMPO retrievals, and data evaluation techniques applied during this study. Section 3
103 provides the results of the comparison of the TB-Clim and modeled a priori profile products with TOLNet observations
104 and the impact of each product, when applied as a priori, on TEMPO tropospheric O₃ profile retrievals. Finally, Sect.
105 4 concludes this study.

106 **2 Data and methods**

107 **2.1 TOLNet**

108 TOLNet provides Differential Absorption Lidar (DIAL)-derived vertically-resolved O₃ mixing ratios at 6 different
109 locations of North America (<http://www-air.larc.nasa.gov/missions/TOLNet/>). TOLNet data have been used

110 extensively in atmospheric chemistry research on topics such as STE, air pollution transport, nocturnal O₃
111 enhancements, PBL pollution entrainment, source attribution of O₃ lamina, and the impact of wildfire and lightning
112 NO_x on tropospheric O₃ (e.g., Kuang et al., 2011; Sullivan et al., 2015a, 2016, Johnson et al., 2016; Granados-Muñoz
113 et al., 2017; Langford et al., 2017). Uncertainty in TOLNet O₃ measurements due to systematic error are approximately
114 4-5% for all instruments at all altitudes. Precision will vary from 0% to > 20% and is dependent on individual
115 instrument characteristics, time of day, and temporal and vertical averaging (precision typically degrades with height
116 for altitudes above 8-10 km) (Kuang et al., 2013; Sullivan et al., 2015b; Leblanc et al., 2016). Since TOLNet
117 observations used during this study are hourly-averaged and typically below 10 km agl, overall uncertainty can be
118 assumed to be ≤ 10%. TOLNet data were applied in this study to evaluate the TB-Clim and model-predicted profiles
119 which could potentially be used as TEMPO a priori information. Furthermore, theoretical TEMPO O₃ retrievals in the
120 troposphere and LMT were calculated using the climatology/model profiles as a priori with TOLNet data representing
121 the “true” atmospheric O₃ profiles (see Sect. 2.2).

122 During this study, vertical O₃ profiles from 3 separate TOLNet sites during the summer (July-August) of
123 2014 were applied. Figure 1 shows the location of the Goddard Space Flight Center (GSFC) TROPOspheric OZone
124 (TROPOZ), Jet Propulsion Laboratory (JPL) Table Mountain Facility (TMF), and the University of Alabama in
125 Huntsville (UAH) Rocket-city O₃ Quality Evaluation in the Troposphere (RO3QET) TOLNet systems which provided
126 the observations used during this work. These 3 sites were selected due to data availability ([http://www-](http://www-air.larc.nasa.gov/missions/TOLNet/data.html)
127 [air.larc.nasa.gov/missions/TOLNet/data.html](http://www-air.larc.nasa.gov/missions/TOLNet/data.html)) and to represent differing parts of North America, which will be
128 observed by TEMPO, with varying topography, meteorology, and atmospheric chemistry conditions (overview
129 information for each station is presented in Table 1). The RO3QET system is located in the southeast US where the
130 air quality is impacted by both anthropogenic and natural emission sources, complex chemistry, and multiple transport
131 pathways (e.g., Hidy et al., 2014; Johnson et al., 2016; Kuang et al., 2017). During the summer of 2014 this lidar
132 system measured O₃ profiles from the surface to ~5 km agl during the daytime hours. The TROPOZ system, which is
133 typically operated at NASA GSFC, was remotely stationed in Fort Collins, Colorado to support the Deriving
134 Information on Surface Conditions from Column and VERTically Resolved Observations Relevant to Air Quality
135 (DISCOVER-AQ) Colorado and Front Range Air Pollution and Photochemistry Éxperiment (FRAPPÉ) field
136 campaigns between July-August 2014. The TROPOZ system was arranged to take daytime observations of O₃ profiles
137 in the intermountain west region of the US alongside the frontal range of the Rocky Mountains. The air quality of this
138 location is impacted by large anthropogenic emission sources, complex local transport, and common STE events (e.g.,
139 Sullivan et al., 2015a, 2016; Vu et al., 2016). Finally, the TOLNet system at the JPL TMF is representative of the
140 western US and remote high-elevation locations. This location has O₃ profiles largely controlled by long-range
141 transport and STEs typical of remote high-elevation locations in the US (e.g., Granados-Muñoz and Leblanc, 2016;
142 Granados-Muñoz et al., 2017). During the summer of 2014, the JPL TMF lidar only conducted measurements during
143 the nighttime hours and therefore will only be used for daily-averaged comparisons to TB-Clim and model predictions.

144

145

146 2.2 TEMPO O₃ profile retrieval

147 TEMPO will adapt the current SAO OMI UV-only O₃ profile algorithm (Liu et al., 2010) to derive O₃ profiles from
148 joint UV+VIS measurements based on the optimal estimation technique (Rodgers, 2000). Partial O₃ columns at
149 different altitudes, along with other retrieved variables, are iteratively derived by simultaneously minimizing the
150 differences between measured and simulated radiances and between the retrieved and a priori state vectors. For this
151 study, we use the linear estimate approach to perform theoretical TEMPO retrievals and evaluate the impact of a priori
152 profiles on these retrievals. This linear estimation approach is a good first-order approximation of non-linear satellite
153 retrievals and has been used in numerous research studies (e.g., Bowman et al., 2002; Worden et al., 2007; Kulawik
154 et al., 2006, 2008; Natraj et al., 2011; Zoogman et al., 2014). In this approach, shown in Eq. (1), the retrieved O₃
155 profile (X_r) is derived as:

$$156 X_r = X_a + A(X_t - X_a) + G\varepsilon, \quad (1)$$

157 where X_a is the a priori O₃ profile, A is the averaging kernel (AK) matrix, X_t is the true O₃ profile, G is the gain matrix,
158 and ε is the measurement noise. The last term on the right represents the retrieval precision. During this study, no
159 measurement noise/error is taken into account. The error component adds measurement noise to the linear retrievals,
160 however, neglecting this term does not affect the inter-comparison of the impact of individual a priori sources on
161 TEMPO retrieved tropospheric O₃.

162 2.2.1 TEMPO averaging kernels

163 The UV+VIS AKs applied during this study are based on TEMPO retrieval sensitivity studies that play a key role in
164 determining the instrument requirements and verification of the retrieval performance (Zoogman et al., 2017). The
165 production of these AKs involved: 1) radiative transfer model simulations of TEMPO radiance spectra and weighting
166 functions, 2) retrieval AKs and errors constrained by the TB-Clim a priori mean and error covariance matrix, and 3)
167 measurement errors estimated using the TEMPO signal to noise ratio model. To represent TEMPO hourly
168 measurements throughout the year, the retrieval sensitivity calculation was performed hourly for 12 days (15th day of
169 each month) over the TEMPO domain at a spatial resolution of 2.0°×2.5° (latitude × longitude) using hourly GEOS-
170 Chem model fields. For detailed information about the TEMPO retrieval sensitivity studies, and the input variables,
171 used to derive AKs applied during this study see Zoogman et al. (2017). During this study, we used the UV+VIS O₃
172 retrieval AKs corresponding to the month and location of TOLNet systems representative of near clear-sky conditions.
173 Figure 2 shows an example of the UV+VIS AK matrix at the UAH RO3QET site for 20 UTC in August. The enhanced
174 sensitivity of TEMPO retrievals in the lower troposphere, in particular the lowest ~2 km, is demonstrated by the large
175 values of A (normalized to 1 km, degrees of freedom (DFS) per km) in Fig. 2 (> 0.20). When including VIS with UV
176 wavelengths, O₃ retrievals can be greater than a factor of 2 more sensitive in the first 2 km of the troposphere in
177 comparison to just using UV wavelengths. This is particularly important as accurate O₃ observations between 0-2 km
178 agl is a key requirement of TEMPO to be a sufficient data source for air quality research/monitoring (Zoogman et al.,
179 2017).

180 2.2.2 TB-Clim

181 During this study, TB-Clim is evaluated with observations to determine the ability of these profiles to represent the
182 spatio-temporal variability of tropospheric O₃ in North America. A detailed description of the data and procedures
183 used to derive TB-Clim can be found in Bak et al. (2013). The climatology provides monthly-averaged O₃ profiles
184 with 1 km vertical resolution relative to the tropopause in 18 10°-latitude bins (Bak et al., 2013). During this study,
185 hourly TB-Clim O₃ profiles were derived by applying hourly-averaged GEOS-5 FP tropopause heights. Figure 3
186 illustrates the monthly-averaged vertical structure of TB-Clim that will be evaluated at the RO3QET, TROPOZ, and
187 JPL TMF system locations representative of various regions of the US in July-August 2014. At the location of the
188 RO3QET system (Fig. 3, green line), O₃ values are ~55 ppb near the surface during July and August and steadily
189 increase to ~95 ppb at 10 km. For the location of the TROPOZ system (Fig. 3, black line), O₃ values are ~40-45 ppb
190 near the surface and increase to ~80 ppb at 10 km. Finally, at the location of the JPL TMF lidar system (Fig. 3, red
191 line), O₃ values are ~50-55 ppb near the surface and increase to 80-95 ppb at 10 km.

192 2.3 Simulated O₃ profile data

193 Satellite O₃ retrieval algorithms typically apply climatologies derived from observational data (i.e., ozonesondes) as
194 a priori information (Liu et al., 2005, 2010; Cai et al., 2012). However, some satellites, such as TES operational
195 retrievals, apply climatological O₃ profiles from global CTMs as a priori information (Worden et al., 2007). During
196 this work, we evaluate time-specific O₃ profile information from a NRT operational data assimilation model (GEOS-
197 5 FP), reanalysis model (MERRA2), and a CTM (GEOS-Chem) using TOLNet data and investigate how these model
198 products impact theoretical TEMPO O₃ retrievals when applied as a priori information. Due to numerous reasons the
199 standard TEMPO O₃ profile algorithm will need to apply an hourly-resolved monthly mean climatology, however, we
200 evaluated time-specific model data here as TEMPO data users can simply apply the outputs from the standard retrieval
201 to recalculate the tropospheric O₃ vertical profiles using a different source of a priori. These simulated products were
202 selected to represent model predictions of O₃ with highly varying complexity in atmospheric chemistry calculations,
203 emissions information, data assimilation techniques, and spatial resolution.

204 2.3.1 GEOS-5 FP and MERRA2

205 The GEOS-5 atmospheric general circulation model (AGCM) and data assimilation system (DAS) is a product of the
206 GMAO and is described in Rienecker et al. (2008) with most recent updates presented in Molod et al. (2012). Aerosol
207 and trace gases are transported in the GEOS-5 AGCM using a finite-volume dynamics scheme implemented with
208 various physics packages (Putman and Lin, 2007; Bacmeister et al., 2006) and turbulently mixed using the Lock et al.
209 (2000) PBL scheme. The GEOS-5 AGCM ADS assimilates roughly 2×10^6 observations for each analysis using the
210 Gridpoint Statistical Interpolation (GSI) three-dimensional variational (3DVar) analysis technique (Wu et al., 2002).
211 A product from the GEOS-5 AGCM is the operationally provided GEOS-5 FP data which offers NRT DAS predictions
212 (typically within 24 hours) of O₃ vertical profiles at a $0.25^\circ \times 0.3125^\circ$ spatial resolution and 72 vertical levels.
213 Additionally, we apply MERRA2 reanalysis O₃ profiles which are also produced using the GEOS-5 AGCM (Molod
214 et al., 2012) and provided at a $0.50^\circ \times 0.667^\circ$ spatial resolution and 72 vertical levels. Both GEOS-5 FP and MERRA2

215 O₃ vertical profiles are driven by the assimilation of OMI and Microwave Limb Sounder (MLS) satellite data.
216 Predictions of O₃ from these products are most trusted in the upper troposphere and stratosphere due to OMI and MLS
217 having limited sensitivity in the lower troposphere (e.g., Wargan et al., 2015; Ott et al., 2016). The work by Wargan
218 et al. (2015) shows that due to highly simplified atmospheric chemistry and lack of surface emissions in the GEOS-5
219 AGCM, O₃ predictions in the middle to lower troposphere tend to be biased. However, during this work these 3 hour-
220 averaged products are applied to understand how NRT DAS and reanalysis models could be used as a priori
221 information in TEMPO O₃ retrievals.

222 2.3.2 GEOS-Chem

223 GEOS-Chem (v9-02) was applied in this work as a proxy to determine how a full CTM or air quality model could
224 potentially be used as a priori information in TEMPO O₃ retrievals. The purpose of this work is not to evaluate the
225 performance of the GEOS-Chem model, or to suggest GEOS-Chem as the only model to provide a priori information
226 for TEMPO, but to simply evaluate how CTM predictions impact the accuracy of theoretical TEMPO O₃ retrievals.
227 The CTM is driven by GEOS-5 FP meteorological data in a nested regional mode for July and August 2014, after a
228 2-month spin-up period, at a 0.25°×0.3125° spatial resolution and 47 hybrid terrain following vertical levels for the
229 North American domain (130°-60°W, 9.75°-60°N). GEOS-Chem includes detailed O₃-NO_x-hydrocarbon-aerosol
230 chemistry coupled to H₂SO₄-HNO₃-NH₃ aerosol thermodynamics (Bey et al., 2001). Furthermore, aerosol and trace
231 gas transport are calculated using the TPCORE parameterization (Lin and Rood, 1996) and dry and wet deposition
232 (Wang et al., 1998; Amos et al., 2012) is simulated on a 10-minute time-step. A detailed description of the version of
233 GEOS-Chem, and emission inventories, applied during this study can be found in Johnson et al. (2016).

234 2.4 Data evaluation

235 The evaluation of TB-Clim and model O₃ profiles was done for summer-, daytime- (6am - 6pm local time), and hourly-
236 averages at the RO3QET and TROPOZ system locations during July and August 2014. Due to the hours of operation,
237 the evaluation at the JPL TMF lidar location was not conducted for hourly-averages and is only applied for summer-
238 and daily-averages. To determine the ability of a NRT DAS, reanalysis, and CTM model to replicate TOLNet-
239 observed O₃, GEOS-5 FP, MERRA2, and GEOS-Chem data will be evaluated simultaneously with TB-Clim. For all
240 evaluation and inter-comparisons, TB-Clim, model data, TOLNet observations, and TEMPO calculations are hourly-
241 averaged and averaged/interpolated to the vertical grid of the TEMPO AKs during all times/locations when/where
242 TOLNet measurements were obtained. TB-Clim and model data used as a priori and resulting X_r calculations will be
243 evaluated using statistical parameters (correlation (R), bias, bias standard deviation (1σ), mean normalized bias
244 (MNB), root mean squared error (RMSE)) and time-series analysis for tropospheric (0-10 km, 0-5 km for RO3QET)
245 and LMT (0-2 km) columns. Tropospheric column values are considered to extend from the surface to 10 km in this
246 study based on the fact that TOLNet systems typically only measured to ~10 km agl.

247

248 **3 Results**

249 **3.1 Evaluation of TB-Clim and model-predicted tropospheric O₃ profiles**

250 In terms of summertime-averaged tropospheric O₃ profiles, TB-Clim and the GEOS-5 FP, MERRA2, and GEOS-
251 Chem models could generally replicate the vertical structure of tropospheric O₃ measured by TOLNet lidars. However,
252 the evaluation of these products as a priori in TEMPO O₃ retrievals at a seasonal/monthly average is insufficient as
253 TEMPO will provide hourly, high spatial resolution, tropospheric and LMT O₃ values. Therefore, in the following
254 sections we evaluate these products for daily- and hourly-averages to focus on inter-daily and diurnal variability.

255 **3.1.1 Daily-averaged tropospheric O₃ profiles**

256 This section focuses on evaluating the ability of TB-Clim and the GEOS-5 FP, MERRA2, and GEOS-Chem models
257 to reproduce observed daily variability of O₃ in the troposphere and near the surface. Figure 4 shows the daily-averaged
258 tropospheric and LMT O₃ columns from TB-Clim and models compared to that observed by TOLNet at all 3 sites
259 with comparison statistics displayed in Table 2. Some slight inter-daily variability can be seen in TB-Clim tropospheric
260 O₃ due to varying time-dependent tropopause heights, however, the variability in LMT values is mostly due to only
261 sampling values in the vertical layers and times when TOLNet observations were obtained (vertical layers of TOLNet
262 observations varied between hours and days). Due to the zonal and monthly mean nature of TB-Clim, this dataset is
263 unable to replicate inter-daily O₃ observations consistently displaying low and negative correlation values with daily
264 TOLNet observations in the troposphere (R range between -0.09 and -0.35) and near the surface (R range between -
265 0.15 and -0.68). The models demonstrate a better ability to replicate the daily variability of observed tropospheric O₃
266 at the TOLNet system locations. Overall, CTM predictions from GEOS-Chem was the only source of O₃ profiles
267 which consistently displayed moderate to high positive correlation (all R values > 0.47) compared to all TOLNet
268 observations in the troposphere and near the surface. This result is not overly surprising as a full CTM includes aspects
269 necessary to reproduce the spatio-temporal tropospheric O₃ variability occurring in nature such as data-assimilated
270 meteorological fields, comprehensive atmospheric chemistry mechanisms, and state-of-the-art trace gas and aerosol
271 emissions data.

272 Figure 4a, b shows larger variability of daily-averaged LMT O₃ (44 to 68 ppb) from the RO3QET system
273 than that in the tropospheric column (48 to 64 ppb). From Table 2 it can be seen that TB-Clim was generally high
274 compared to lidar-measured tropospheric O₃ mixing ratios (average bias = 3.7 ppb) with large bias standard deviations
275 and RMSE values (> 6 ppb). MERRA2 displayed good agreement in tropospheric O₃ (negative bias ~0.7 ppb) while
276 GEOS-5 FP and GEOS-Chem resulted in moderate high biases (average bias 2.8 and 1.7 ppb, respectively). GEOS-
277 Chem had moderate high biases but with smaller bias standard deviation and RMSE values (< 4.5 ppb) in comparison
278 to the other products due to the ability to better capture inter-daily tropospheric O₃ variability (R = 0.61). LMT O₃
279 observations by the RO3QET lidar were best replicated by the CTM product resulting in the smallest average bias (-
280 1.3 ppb) and bias standard deviation and RMSE values (4.4 ppb) compared to the other products. MERRA2 was
281 consistently low compared to LMT O₃ observations (bias = -4.9 ppb) while TB-Clim and GEOS-5 FP resulted in
282 moderate biases (2.9 and -2.9 ppb, respectively) with all of these products having large bias standard deviations and
283 RMSE (≥ 8.0 ppb).

284 At the TROPOZ system location, large variability in tropospheric (47 to 83 ppb) and LMT O₃ values (41 to
285 73 ppb) was observed. From Fig. 4c, d and Table 2 it can be seen that TB-Clim is unable to replicate the inter-daily
286 tropospheric O₃ variability and is generally higher in comparison to observations with large bias standard deviations
287 (bias ± standard deviation = 2.2 ± 9.7 ppb). GEOS-Chem best replicates the daily variability of tropospheric O₃ with
288 the largest correlation (R = 0.82) and small average bias and standard deviations (2.4 ± 6.0 ppb). GEOS-5 FP and
289 MERRA2 data displayed low positive correlations (R < 0.40) and larger average biases and standard deviations 3.3 ±
290 10.0 and -4.6 ± 9.1 ppb, respectively. In comparison to TROPOZ LMT O₃ observations, TB-Clim and all model
291 products displayed large negative biases. The TB-Clim product resulted in the largest negative biases and bias standard
292 deviations compared to LMT O₃ observations (-11.1 ± 7.5 ppb) and model products displayed smaller biases and
293 standard deviations. GEOS-5 FP data displayed the lowest average bias (-4.4 ppb) compared to TROPOZ
294 observations, however, was unable to replicate the inter-daily variability of LMT O₃ (R = -0.09) resulting in large bias
295 standard deviations (7.3 ppb). Overall, GEOS-Chem was the only product which was able to capture the inter-daily
296 variability of LMT O₃ (R = 0.47) resulting in moderate low biases and the lowest bias standard deviation (-6.7 ± 6.2
297 ppb).

298 Figure 4e, f illustrates that large inter-daily variability of tropospheric (46 to 129 ppb) and LMT (35 to 76
299 ppb) column O₃ was observed at the JPL TMF site during the summer of 2014. This figure and Table 2 shows that
300 TB-Clim is able to represent the average magnitude of tropospheric O₃ (bias = 0.3 ppb) but with large bias standard
301 deviation and RMSE values (>18 ppb) due to the inability to replicate observed inter-daily variability (R = -0.35). The
302 GEOS-Chem model also captures the average magnitude of tropospheric O₃ (bias = -0.5 ppb) but with smaller bias
303 standard deviations (14.6 ppb) compared to TB-Clim due to the ability to replicate the inter-daily availability (R =
304 0.72). GEOS-5 FP and MERRA2 demonstrated negative biases compared to JPL TMF lidar observed tropospheric O₃
305 (-5.0 and -10.6 ppb, respectively) with relatively low bias standard deviations (~13-14 ppb) compared to the other
306 products. The large RMSE values for all products is due to the very large variability in daily-averaged O₃ observations
307 which was not well captured by all products. Near the surface, the GEOS-Chem model clearly best captures the
308 variability of daily-averaged LMT O₃ indicated by the smallest bias and standard deviations (0.9 ± 10.4 ppb) and
309 RMSE (~10.25 ppb) values.

310 3.1.2 Diurnal cycle of tropospheric O₃ profiles

311 TEMPO retrievals will produce hourly tropospheric and LMT O₃ values each day for the entire North America
312 domain. Therefore, this section focuses on evaluating the ability of TB-Clim and the GEOS-5 FP, MERRA2, and
313 GEOS-Chem models to reproduce the observed diurnal variability of O₃ measured at the RO3QET and TROPOZ
314 system locations in the troposphere and near the surface. Figure 5 shows the average diurnal time-series of hourly-
315 averaged tropospheric and LMT O₃ (from all days of observation) from the O₃ climatology and models compared to
316 that observed during the summer of 2014 (statistics displayed in Table 3).

317 Figure 5a, b shows that larger diurnal variability of O₃ was observed for LMT values (48 to 59 ppb) compared
318 to tropospheric values (55 to 60 ppb) at the RO3QET lidar location. All the sources of O₃ profiles evaluated here,
319 excluding the CTM predictions, demonstrate very little diurnal variation in tropospheric and LMT O₃ at the RO3QET

320 lidar location. The GEOS-Chem model was the only product able to replicate the diurnal variability of observed
321 tropospheric O₃ (R = 0.68). MERRA2 resulted in the lowest bias (-1.2 ppb), GEOS-5 FP and GEOS-Chem displayed
322 modest biases (~2.0-2.5 ppb), and TB-Clim had the largest bias (3.5 ppb) compared to RO3QET tropospheric O₃ data.
323 Diurnal RO3QET LMT O₃ data was best replicated by CTM predictions resulting in the highest correlation (R = 0.76),
324 lowest bias and standard deviations (0.3 ± 2.6 ppb), and RMSE values (2.45 ppb). The TB-Clim product resulted in
325 modest biases compared to LMT O₃ data (1.9 ppb) while GEOS-5 FP and MERRA2 were consistently low (negative
326 bias > 3.0 ppb).

327 Figure 5c, d shows the diurnal variability of O₃ that was observed for tropospheric and LMT column values
328 at the TROPOZ lidar location. In the troposphere, O₃ values varied between ~58 to 69 ppb with largest values
329 occurring in the afternoon. Larger diurnal variability was observed near the surface with LMT O₃ values ranging from
330 ~56 to 75 ppb with largest values occurring between 21 and 05 UTC. GEOS-Chem data is the only product which
331 could replicate the diurnal variability of TROPOZ lidar tropospheric O₃ observations (R = 0.78). The TB-Clim, GEOS-
332 5 FP, and GEOS-Chem products demonstrate moderate high biases (2.2-3.3 ppb) compared to the observations while
333 MERRA2 was consistently low (bias = -5.1 ppb). For comparison of near-surface O₃ values (see Fig. 5d), none of the
334 products sufficiently captured the magnitude and degree of diurnal variability of LMT O₃ at the TROPOZ lidar
335 location. The TB-Clim product displayed a small positive correlation (R = 0.26) and large negative biases (-12.6 ppb),
336 bias standard deviation (6.9 ppb), and RMSE values (14.25 ppb). The GEOS-5 FP and GEOS-Chem models display
337 the lowest bias (negative bias between 7.5 ppb and 7.7 ppb), however, the CTM is more highly correlated (R = 0.92)
338 and resulted in lower bias standard deviations (4.8 ppb) and RMSE values (9.01 ppb). This indicates that while no
339 product reproduced the magnitude or degree of diurnal variability of near-surface O₃ observed by the TROPOZ lidar,
340 the GEOS-Chem CTM does the best job on average.

341 **3.2 Prior O₃ vertical profile impact on TEMPO retrievals**

342 This section focuses on how the TB-Clim, GEOS-5 FP, MERRA2, and GEOS-Chem O₃ profiles impact theoretical
343 TEMPO tropospheric O₃ profile retrievals when applied as the a priori information in Eq. (1). The evaluation is focused
344 on how different sources of a priori impacted the overall accuracy of TEMPO tropospheric O₃ retrievals and the ability
345 to meet the required precision of tropospheric and LMT O₃ observations of 10 ppb (Zoogman et al., 2017). The
346 requirement for TEMPO tropospheric O₃ is that retrieval errors (root square sum of retrieval precision and smoothing
347 errors) or overall biases should be < 10 ppb, and, therefore, we quantify the number of occurrences when total error
348 or bias standard deviation/RMSE exceeds this 10 ppb limit. TEMPO will provide tropospheric and LMT O₃ at high
349 temporal resolution and therefore, X_r values from Eq. (1), using the individual a priori sources, were evaluated on a
350 daily-averaged and diurnal cycle time scale.

351 **3.2.1 Tropospheric O₃ TEMPO retrievals**

352 Figure 6 shows the time-series of daily-averaged tropospheric and LMT X_r column values and bias calculations when
353 using TB-Clim and model data as a priori information when compared to observed O₃ at all 3 TOLNet sites (statistics
354 in Table 4). When focusing on the accuracy of the theoretical TEMPO retrievals for tropospheric X_r columns (left

355 column in Fig. 6), it can be seen that X_r values using all a priori profiles: 1) are similar, 2) are highly correlated with
356 observations (see Table 4), and 3) compare well to observations with tropospheric X_r values typically falling within
357 the 10 ppb bias requirement at all 3 TOLNet locations. From Table 4 it can be seen that daily-averaged tropospheric
358 column biases exceeded the 10 ppb level on 1 and 2 days when using TB-Clim/GEOS-5 FP and MERRA2 data,
359 respectively, as a priori when compared to TROPOZ observations, and for 1 day at the JPL TMF location when using
360 all O₃ products as a priori.

361 Table 4 illustrates that applying TB-Clim as the a priori resulted in the largest tropospheric column X_r biases
362 and modest bias standard deviations (1.4 ± 2.3 ppb) and the MERRA2 data led to the lowest overall bias and modest
363 bias standard deviation (-0.2 ± 2.5 ppb) at the RO3QET lidar location. Using GEOS-Chem a priori profiles resulted
364 in modest biases and the lowest bias standard deviations (1.0 ± 2.0 ppb) and RMSE values (2.17 ppb). At the TROPOZ
365 system site, the lowest tropospheric column X_r biases and standard deviation were calculated when applying GEOS-
366 Chem as the a priori (-0.5 ± 2.7 ppb). GEOS-5 FP data also resulted in low mean X_r biases but the largest bias standard
367 deviations (-0.6 ± 4.8 ppb) and MERRA2 data led to larger mean X_r biases but lower bias standard deviations ($-2.2 \pm$
368 4.4 ppb). The use of TB-Clim resulted in modest mean bias and standard deviations (-0.9 ± 4.2 ppb). Finally, at the
369 JPL TMF location all a priori profile sources resulted in average tropospheric column X_r biases of < 1.0 ppb, excluding
370 MERRA2 (bias = -1.7 ppb), with similar bias standard deviations and RMSE values (ranging between 3.0 to 4.0 ppb).
371 Much larger daily variability of tropospheric O₃ was observed at the JPL TMF site compared to the other TOLNet
372 system locations and tropospheric column X_r values from theoretical TEMPO retrievals successfully captured this
373 variability using all the sources of a priori information. These results suggest that TEMPO, using UV+VIS
374 wavelengths, will likely be able to accurately retrieve highly variable tropospheric column O₃ magnitudes regardless
375 of the a priori profile used.

376 3.2.2 LMT O₃ TEMPO retrievals

377 The third column of Fig. 6 shows that much larger differences in daily-averaged LMT column X_r values were
378 calculated, compared to tropospheric X_r values, when using different sources of a priori in Eq. (1). From this figure
379 and Table 4 it can be seen that LMT column X_r values better capture the daily variability of near-surface O₃ compared
380 to the a priori profiles, however, noticeable differences in the statistical comparison of LMT column X_r values using
381 different a priori sources are evident. It can be seen from this figure that at the RO3QET site, daily variability of near-
382 surface O₃ are clearly best captured by LMT X_r values using GEOS-Chem CTM a priori profiles. While the TB-Clim
383 product resulted in LMT X_r values with the smallest mean bias (0.2 ppb), it also led to large RMSE values (5.88 ppb)
384 and the largest bias standard deviations (6.1 ppb) (see Table 4). Table 4 illustrates that LMT column X_r values
385 calculated using CTM a priori profiles had modest mean bias (-2.2 ppb) and the lowest bias standard deviations (2.5
386 ppb) and RMSE (3.26 ppb). Applying the GEOS-5 FP and MERRA2 model products as a priori profiles resulted in
387 the largest mean biases in LMT X_r values (negative biases ≥ 3.4 ppb) along with largest RMSE values (≥ 6.0 ppb).
388 From an air quality perspective, it is important to note that LMT column X_r values using a priori data other than
389 GEOS-Chem are unable to replicate the larger surface O₃ values occurring in the southeast US (see Fig. 6). A few
390 LMT O₃ accuracy/precision requirement exceedances were calculated at the RO3QET lidar location using all a priori

391 products except for GEOS-Chem predictions. The ability of GEOS-Chem to best reproduce the magnitude of the daily
392 LMT O₃ variability resulted in LMT X_r values with the smallest RMSE and bias standard deviations, no
393 accuracy/precision requirement exceedances, and the best ability to capture the range in daily observed O₃.

394 At the location of the TROPOZ lidar, it can be seen from Fig. 6 that LMT X_r values, with the use of TB-
395 Clim a priori, are consistently underestimated in comparison to lidar observations. These LMT X_r values have an
396 average negative bias of > 10.0 ppb and largest RMSE values (~13.0 ppb) resulting in 10 days with accuracy/precision
397 requirement exceedances (see Table 4). These large errors are because the a priori profiles provided by TB-Clim are
398 not able to replicate the highly variable vertical O₃ profiles observed at the TROPOZ lidar location. The GEOS-5 FP,
399 MERRA2, and GEOS-Chem models were better able to replicate these highly variable vertical O₃ profiles providing
400 a priori information more accurately representing O₃ in the intermountain west region of the US. This better
401 representation from model data resulted in LMT X_r values with lower negative mean biases (< 6.5 ppb) and smaller
402 RMSE values (< 9.0 ppb) and bias standard deviations (< 6.5 ppb), and also fewer accuracy/precision requirement
403 exceedances. Overall, CTM-predicted a priori information resulted in LMT X_r values with the least bias and bias
404 standard deviation (-4.8 ± 4.8 ppb), RMSE (6.71 ppb), and accuracy/precision exceedances.

405 At the location of the JPL TMF lidar, much larger daily variability in LMT O₃ mixing ratios were observed
406 during the summer of 2014 compared to the other TOLNet systems. LMT X_r values, using all sources of data as a
407 priori information, had difficulty in replicating this large variability (see Fig. 6). From Table 4, it can be seen that
408 despite relatively low biases when using all sources of a priori (< 5.0 ppb), the inability of LMT X_r values to capture
409 the dynamic daily variability resulted in large bias standard deviations and RMSE values (> 12.5 ppb). Furthermore,
410 6-10 accuracy/precision requirement exceedances out of 26 total days were calculated when using all sources of a
411 priori. Despite 6 error exceedances (the least of all profile products), applying GEOS-Chem predictions as a priori
412 information resulted in the lowest mean biases (1.0 ppb) and RMSE values (12.54 ppb). Typically, large
413 underestimations of LMT X_r values occurred when the lidar observed large O₃ enhancements near the surface and
414 significant overestimations of LMT X_r values were calculated when the lidar observed very large O₃ lamina (>150
415 ppb) aloft. This indicates that the shape of the a priori O₃ vertical profile used in TEMPO tropospheric O₃ retrievals
416 are very important in order to capture X_r values for both the tropospheric and LMT column and this will be discussed
417 in Sect. 3.2.3.

418 Figure 6 and Table 4 demonstrate that in general X_r values in the troposphere and near the surface are more
419 accurately retrieved when applying model predictions, and in particular CTM values from GEOS-Chem, at all 3
420 TOLNet system locations. Also, from this figure it can be seen that in general when large daily-averaged LMT O₃
421 mixing ratios are observed (here defined as days with daily-averaged LMT O₃ > 65 ppb), which are important for air
422 quality purposes, LMT X_r values display less bias when applying GEOS-Chem a priori profile information compared
423 to all other products. For the 11 days in which daily-averaged LMT O₃ mixing ratios exceeded 65 ppb, 64%, 9%, and
424 27% of the LMT X_r values had the smallest bias using GEOS-Chem, GEOS-5 FP, and MERRA2 a priori profiles,
425 respectively. This suggests that applying CTM predictions as a priori profile information will allow TEMPO to observe
426 air quality relevant pollution concentrations of LMT O₃ more accurately compared to TB-Clim and models with
427 simplistic/limited atmospheric chemistry schemes and emission inventories evaluated during this work.

428 3.2.3 Importance of a priori vertical profile shape

429 Figure 7 displays examples of why climatological a priori information in theoretical TEMPO retrievals resulted in
430 large daily-averaged LMT column X_r biases. The first example in Fig. 7a shows the daily-averaged vertical profiles
431 of X_a and X_r with the use of TB-Clim and GEOS-Chem a priori on 08 July 2014 at the JPL TMF site when the lidar
432 observed large LMT O_3 values above EPA NAAQS levels. This case study illustrates how CTMs are more likely to
433 be able to replicate surface O_3 enhancements compared to climatological products. The GEOS-Chem a priori
434 information resulted in more accurate TEMPO X_r values for the tropospheric and LMT O_3 column values. When using
435 GEOS-Chem model predictions as a priori information, TEMPO LMT column X_r retrievals (65.1 ppb) were closer in
436 magnitude to observations (70.2 ppb) compared to when using TB-Clim a priori (54.7 ppb). Furthermore, when using
437 GEOS-Chem a priori information, TEMPO retrievals for the troposphere (65.8 ppb) were also more similar in
438 magnitude to lidar observations (64.2 ppb) compared to using a priori data from TB-Clim (68.2 ppb).

439 Another example is illustrated in Fig. 7b which shows X_a and X_r when using TB-Clim and GEOS-5 FP
440 predictions as a priori profiles in TEMPO retrievals on 21 August 2014 at the JPL TMF lidar location. On this day, a
441 STE event was likely occurring as tropospheric O_3 mixing ratios were measured to be > 200 ppb between 6-9 km.
442 This case study illustrates how a NRT DAS model, GEOS-5 FP, displayed some ability to replicate the large O_3 lamina
443 in the middle/upper troposphere due to being constrained with upper atmospheric observations. The GEOS-5 FP a
444 priori information resulted in more accurate TEMPO X_r values for the tropospheric and LMT O_3 column values. When
445 using GEOS-5 FP data as a priori information, TEMPO X_r values for tropospheric O_3 of 130.4 ppb compared closely
446 to the JPL TMF lidar observations (135.6 ppb) while TB-Clim data resulted in much lower values (112.4 ppb).
447 However, the large adjustment needed to correct the a priori profiles to match tropospheric column O_3 observations
448 led to noticeable overestimations of TEMPO LMT X_r values. Since the GEOS-5 FP a priori data was able to better
449 replicate the STE event compared to TB-Clim, the LMT X_r overestimation of observed LMT O_3 values (48.8 ppb) is
450 much less when applying GEOS-5 FP (77.6 ppb) than when applying TB-Clim (99.1 ppb).

451 Overall, these results demonstrate that because TEMPO will only have up to ~ 1.5 DFS in the troposphere
452 (only ~ 0.2 DFS in the 0-2 km level), it is important for a priori profiles to match the general shape of observations,
453 throughout the entire troposphere and LMT, in order to accurately retrieve both total tropospheric and LMT O_3 values.
454 While the magnitude of the tropospheric O_3 column will be largely controlled by the retrieval, the shape of the a priori
455 profile itself will have an impact on the shape of the retrieved tropospheric O_3 profile, and therefore the LMT O_3
456 magnitudes where satellite sensitivity is low.

457 3.2.4 Diurnal cycle of tropospheric TEMPO retrievals

458 This section focuses on evaluating the ability of TEMPO to retrieve hourly-averaged tropospheric O_3 applying TB-
459 Clim and the GEOS-5 FP, MERRA2, and GEOS-Chem models as a priori profile information. This evaluation was
460 conducted for one day each at the RO3QET and TROPOZ sites where constant lidar measurements were obtained in
461 the troposphere/LMT and near-surface O_3 enhancements with potential air quality relevant impacts were observed.
462 Figure 8 shows the time-series of hourly-averaged tropospheric and LMT column X_r retrievals when using TB-Clim
463 and models as a priori compared to that observed by RO3QET on 07 August 2014 and by TROPOZ on 22 July 2014.

464 This figure also displays the a priori vertical O₃ profiles used in TEMPO retrievals for the hour of largest LMT O₃
465 observations from the TOLNet systems (20 UTC at the RO3QET location and 22 UTC at the TROPOZ site location).

466 In comparison to lidar measurements by RO3QET, TEMPO retrievals, with all sources of a priori profiles,
467 are able to reproduce the diurnal pattern of tropospheric and LMT column O₃ values (all R values > 0.98) (see Table
468 5 and Fig. 8). Table 5 shows that all a priori products resulted in TEMPO retrieving average tropospheric column O₃
469 with minimal biases, however, GEOS-Chem was the only product which resulted in LMT X_r values comparable to
470 observations. This is because GEOS-Chem a priori profiles allow for more dynamic O₃ retrievals for the entire
471 troposphere and LMT. This is demonstrated by the fact that the daily-mean and standard deviation (1σ) of hourly LMT
472 O₃ from TEMPO using GEOS-Chem a priori information (62.1 ± 5.4 ppb) compared the closest to RO3QET
473 observations (65.2 ± 9.3 ppb). The daily-mean and standard deviations for LMT X_r retrievals, using the other a priori
474 profiles, underpredicted the magnitude and diurnal variability to a higher degree compared to predictions using GEOS-
475 Chem a priori.

476 Similar results are displayed in Fig. 8 and Table 5 when evaluating the case study at the TROPOZ site
477 location. Once again, TEMPO retrievals with all sources of a priori profiles are generally able to reproduce the diurnal
478 pattern of tropospheric and LMT column O₃ values (all R values ≥ 0.51) but all show large negative biases compared
479 to LMT observations. These low biases are likely due to the very large LMT O₃ values measured by TROPOZ on this
480 day associated with complex vertical/horizontal transport (Sullivan et al., 2016) which were not well reproduced by a
481 priori products evaluated during this study. However, Table 5 shows that GEOS-Chem model a priori data resulted in
482 TEMPO retrievals of hourly tropospheric and LMT O₃ with the least bias. LMT X_r values using the TB-Clim, GEOS-
483 5 FP, and MERRA2 a priori information displayed too little diurnal variability (nearly a factor of 2 lower standard
484 deviation compared to TEMPO retrievals using GEOS-Chem a priori data) and a consistent underestimate of
485 observations. During both case studies, a priori profile shape was critical for TEMPO retrievals to accurately retrieve
486 both tropospheric and LMT O₃. Figure 8 shows a priori profiles from all products for the hour of each day where
487 largest LMT O₃ observations occurred. This figure further emphasizes that GEOS-Chem CTM simulations are able to
488 better capture the dynamic vertical O₃ profiles observed by the lidars compared to the other a priori profile sources.
489 While the GEOS-Chem X_a profiles underestimate the large LMT O₃ enhancements, the ability to replicate the general
490 shape greatly improves tropospheric and LMT column TEMPO X_r values.

491 **4 Conclusions**

492 This study evaluated the a priori vertical O₃ profile product currently suggested to be used in TEMPO tropospheric
493 profile retrievals (TB-Clim, Zoogman et al., 2017) and simulated profiles from operational (GEOS-5 FP), reanalysis
494 (MERRA2), and CTM predictions (GEOS-Chem). The spatio-temporal representativeness of the vertical profiles from
495 each product was evaluated using TOLNet lidar observations of tropospheric O₃ during the summer (July-August) of
496 2014. The TOLNet sites used in this study are situated in areas which represent the southeastern US (RO3QET),
497 intermountain west (TROPOZ), and remote high-elevation locations in the western US (JPL TMF). Because TEMPO
498 will provide high spatial resolution tropospheric (0-10 km) and LMT (0-2 km) O₃ values on an hourly time scale,

499 potential sources of a priori profiles must be able to replicate inter-daily variability and the diurnal cycle of observed
500 vertical tropospheric O₃ profiles.

501 When evaluating summertime-averaged tropospheric O₃ profiles, it was found that TB-Clim, GEOS-5 FP,
502 MERRA2, and GEOS-Chem data could generally replicate the vertical structure of tropospheric O₃ measured by
503 TOLNet lidars. However, the seasonal/monthly evaluation is insufficient as TEMPO will provide hourly, high spatial
504 resolution, tropospheric and LMT O₃ values. The evaluation of daily-averaged tropospheric and LMT column O₃
505 values from these products using lidar observations resulted in varying statistical comparisons. Overall, at all 3
506 TOLNet system locations, GEOS-Chem provided the only data product which consistently captured the inter-daily
507 variability of tropospheric and LMT column O₃ observations. Furthermore, due to the monthly- and zonal-mean nature
508 of TB-Clim, this product was unable to reproduce the inter-daily variability of tropospheric O₃. The ability of the
509 models, in particular GEOS-Chem, to better replicate the temporal variability of O₃ observations led to better statistical
510 comparison to daily-averaged TOLNet data. An important fact demonstrated in this study is that models, primarily
511 GEOS-Chem CTM predictions, displayed better skill in reproducing the largest peaks in daily-averaged near surface
512 O₃ observations which have important implications for air quality. This is partially because GEOS-Chem data best
513 replicated the diurnal cycle of observations of tropospheric and LMT column O₃ from observations. Overall, the
514 GEOS-Chem CTM predictions had the best statistical comparison to daily- and hourly-averaged tropospheric and
515 LMT column O₃ observations.

516 The impact of different a priori profile products on TEMPO tropospheric O₃ retrievals was evaluated during
517 this study. The results demonstrate that since TEMPO will only have up to ~1.5 DFS in the troposphere (and ~0.2 in
518 the 0-2 km column), the ability of the a priori profile to replicate the general shape of the “true” O₃ vertical structure
519 (throughout the entire troposphere and LMT) is important in order for the sensor to accurately retrieve both
520 tropospheric column and near surface O₃ values. In general, the magnitude of the tropospheric O₃ column from
521 TEMPO will be largely controlled by the retrieval and the shape of the a priori profile will have a noticeable impact
522 on the shape of the retrieved tropospheric O₃ profile, and therefore the LMT O₃ magnitudes where satellite sensitivity
523 is low. This was demonstrated as TEMPO X_r values, using all a priori data, were able to accurately retrieve highly
524 variable column tropospheric O₃ magnitudes, however, large differences in LMT X_r values were calculated. In
525 general, LMT column X_r values were more accurately retrieved with model a priori profiles, especially with GEOS-
526 Chem predictions. The better performance of TEMPO LMT X_r values, with GEOS-Chem a priori profiles, is because
527 it better reproduces the dynamic vertical structures and inter-daily/diurnal variability of tropospheric O₃. Most
528 importantly from an air quality perspective is that when large daily-averaged LMT O₃ mixing ratios were observed,
529 X_r values near the surface with GEOS-Chem a priori displayed the least bias. Overall, this study suggests that applying
530 a CTM as a priori will likely allow TEMPO retrievals to observe air quality relevant O₃ concentrations more accurately
531 than TB-Clim and other models with limited atmospheric chemistry schemes and emission inventories.

532 This study is a first step in determining the impact of varying a priori profile sources on the accuracy of
533 TEMPO tropospheric and LMT column O₃ retrievals in North America. The results demonstrate that model
534 simulations, in particular those from a CTM, improve TEMPO tropospheric O₃ retrievals over climatological products
535 such as TB-Clim when applied as the a priori. However, there are instances where CTM predictions did not improve

536 TEMPO retrieved values compared to the TB-Clim data. Furthermore, out of the 59 total days of TOLNet observations
537 analyzed during this study, LMT column X_T values using GEOS-Chem a priori profiles show biases greater than the
538 TEMPO 10 ppb accuracy requirement for ~15% of the days. It should be noted that this number of LMT column X_T
539 error exceedances is the least compared to when using all the sources of a priori and greater than a factor of 2 smaller
540 than when applying TB-Clim a priori. The main reason for the majority of error exceedances is because the a priori
541 profiles do not capture the dynamic vertical O_3 profile observed by the TOLNet lidars.

542 The results of this study clearly demonstrate that using simulated time-specific (non-climatological) O_3
543 profile data will improve near-surface TEMPO O_3 retrievals, however, implementing NRT daily/hourly predictions
544 from CTM or air quality models as the a priori is best suited for using TEMPO data to study topics such as air quality
545 or event-based processes (e.g., air quality exceedances, wildfires, stratospheric intrusions, pollution transport, etc.).
546 Applying time-specific daily/hourly predictions from CTM or air quality models as the a priori will impact
547 errors/uncertainties and long-term trends in tropospheric O_3 retrievals from TEMPO and these impacts would be
548 difficult to separate from actually retrieved information. Therefore, the standard TEMPO O_3 profile algorithm will
549 need to use an hourly-resolved monthly mean climatology and follow-on studies to this manuscript are currently being
550 conducted to develop different CTM-simulated O_3 climatology products and test them in the retrieval algorithm. It is
551 important to note that TEMPO data users can easily apply the output from the standard retrieval (e.g., original a priori
552 O_3 profile, retrieved O_3 profile, and AKs) and recalculate the tropospheric O_3 vertical profiles using a new/different
553 source of a priori following the methods of this study. This will allow data users to apply a priori profiles they believe
554 will result in the most accurate/representative tropospheric and LMT O_3 magnitudes from TEMPO without having to
555 rerun the computationally-expensive SAO retrieval algorithm.

556 *Acknowledgements.* This work is supported by the TOLNet program within NASA's Science Mission Directorate. X.
557 Liu and P. Zoogman were supported by the NASA Earth Venture Instrument TEMPO project (NNL13AA09C). The
558 authors would also like to thank the Harvard University Atmospheric Chemistry Modeling Group for providing the
559 GEOS-Chem model and the NASA GMAO for providing the GEOS-5 FP and MERRA2 products used during our
560 research. Resources supporting this work were provided by the NASA High-End Computing (HEC) Program through
561 the NASA Advanced Supercomputing (NAS) Division at NASA Ames Research Center. All the authors express
562 gratitude to the support from NASA's Earth Science Division at Ames Research Center. Finally, the views, opinions,
563 and findings contained in this report are those of the authors and should not be construed as an official NASA or
564 United States Government position, policy, or decision.

565 **References**

- 566 Amos, H. M., Jacob, D. J., Holmes, C. D., Fisher, J. A., Wang, Q., Yantosca, R. M., Corbitt, E. S., Galarneau, E.,
567 Rutter, A. P., Gustin, M. S., Steffen, A., Schauer, J. J., Graydon, J. A., St. Louis, V. L., Talbot, R. W., Edgerton,
568 E. S., Zhang, Y., and Sunderland, E. M.: Gas-particle partitioning of atmospheric Hg(II) and its effect on global
569 mercury deposition, *Atmos. Chem. Phys.*, 12, 591-603, <https://doi.org/10.5194/acp-12-591-2012>, 2012.
- 570 Atkinson, R.: Gas-phase Tropospheric Chemistry of Organic Compounds: A Review, *Atmos. Environ.*, 26, 1, 1-41,
571 doi:10.1016/0960-1686(90)90438-S, 1990.
- 572 Bacmeister, J. T., Suarez, M. J., and Robertson, F. R.: Rain Re-evaporation, Boundary Layer Convection Interactions,
573 and Pacific Rainfall Patterns in an AGCM, *J. Atmos. Sci.*, 63, 3383-3403, <https://doi.org/10.1175/JAS3791.1>,
574 2006.
- 575 Bak, J., Liu, X., Wei, J. C., Pan, L. L., Chance, K., and Kim, J. H.: Improvement of OMI ozone profile retrievals in
576 the upper troposphere and lower stratosphere by the use of a tropopause-based ozone profile climatology, *Atmos.*
577 *Meas. Tech.*, 6, 2239-2254, <https://doi.org/10.5194/amt-6-2239-2013>, 2013.
- 578 Bak, J., Liu, X., Kim, J.-H., Haffner, D. P., Chance, K., Yang, K., and Sun, K.: Characterization and correction of
579 OMPS nadir mapper measurements for ozone profile retrievals, *Atmos. Meas. Tech.*, 10, 4373-4388,
580 <https://doi.org/10.5194/amt-10-4373-2017>, 2017.
- 581 Beer, R.: TES on the aura mission: scientific objectives, measurements, and analysis overview, *IEEE Trans. Geosci.*
582 *Remote Sens.*, 44, 1102-1105, doi:10.1109/TGRS.2005.863716, 2006.
- 583 Bey, I., Jacob, D. J., Yantosca, R. M., Logan, J. A., Field, B., Fiore, A. M., Li, Q., Liu, H., Mickley, L. J., and Schultz,
584 M.: Global modeling of tropospheric chemistry with assimilated meteorology: Model description and evaluation,
585 *J. Geophys. Res.*, 106, 23073-23095, doi:10.1029/2001JD000807, 2001.
- 586 Bowman, K. W., Rodgers, C. D., Kulawik, S. S., Worden, J., Sarkissian, E., Osterman, G., Steck, T., Lou, M.,
587 Eldering, A., Shephard, M., Worden, H., Lampel, M., Clough, S., Brown, P., Rinsland, C., Gunson, M., and Beer,
588 R.: Tropospheric Emission Spectrometer: retrieval method and error analysis, *IEEE Trans. Geosci. Remote Sens.*,
589 44, 1297-1307, doi:10.1109/TGRS.2006.871234, 2006.
- 590 Cai, Z., Liu, Y., Liu, X., Chance, K., Nowlan, C. R., Lang, R., Munro, R., and Suleiman, R.: Characterization and
591 correction of Global Ozone Monitoring Experiment 2 ultraviolet measurements and application to ozone profile
592 retrievals?, *J. Geophys. Res.*, 117, D07305, doi:10.1029/2011JD017096, 2012.
- 593 Chance, K., Liu, X., Suleiman, R. M., Flittner, D. E., Al-Saadi, J., and Janz, S. J.: Tropospheric emissions: Monitoring
594 of pollution (TEMPO), *Earth Observing Systems XVIII*, Paper 88660D, doi:10.1117/12.2024479, 2013.
- 595 Duncan, B. N., Prados, A. I., Lamsal, L. N., Liu, Y., Streets, D. G., Gupta, P., Hilsenrath, E., Kahn, R. A., Nielsen, J.
596 E., Beyersdorf, A. J., Burton, S. P., Fiore, A. M., Fishman, J., Henze, D. K., Hostetler, C. A., Krotkov, N. A., Lee,
597 P., Lin, M. Y., Pawson, S., Pfister, G., Pickering, K. E., Pierce, R. B., Yoshida, Y., and Ziemba, L. D.: Satellite
598 data of atmospheric pollution for US air quality applications: Examples of applications, summary of data end-user
599 resources, answers to FAQs, and common mistakes to avoid, *Atmos. Environ.*, 94, 647-662,
600 doi:10.1016/j.atmosenv.2014.05.061, 2014.

601 Fishman, J., Bowman, K. W., Burrows, J. P., Richter, A., Chance, K. V., Edwards, D. P., Martin, R. V., Morris, G.
602 A., Pierce, R. B., Ziemke, J. R., Al-Saadi, J. A., Creilson, J. K., Schaack, T. K., and Thompson, A.M.: Remote
603 sensing of tropospheric pollution from space, *Bulletin of the American Meteorological Society*, 89, 805-821,
604 <https://doi.org/10.1175/2008BAMS2526.1>, 2008.

605 Granados-Muñoz, M. J. and Leblanc, T.: Tropospheric ozone seasonal and long-term variability as seen by lidar and
606 surface measurements at the JPL-Table Mountain Facility, California, *Atmos. Chem. Phys.*, 16, 9299-9319,
607 doi:10.5194/acp-16-9299-2016, 2016.

608 Granados-Muñoz, M. J., Johnson, M. S., and Leblanc, T.: Influence of the North American monsoon on Southern
609 California tropospheric ozone levels during summer in 2013 and 2014, *Geophys. Res. Lett.*, 44, 6431-6439,
610 doi:10.1002/2017GL073375, 2017GL073375, 2017.

611 Hidy, G. M., Blanchard, C. L., Baumann, K., Edgerton, E., Tanenbaum, S., Shaw, S., Knipping, E., Tombach, I.,
612 Jansen, J., and Walters, J.: Chemical climatology of the southeastern United States, 1999-2013, *Atmos. Chem.*
613 *Phys.*, 14, 11893-11914, doi:10.5194/acp-14-11893-2014, 2014.

614 Johnson, M. S., Kuang, S., Wang, L., and Newchurch, M. J.: Evaluating Summer-Time Ozone Enhancement Events
615 in the Southeast United States, *Atmosphere*, 7, 108, doi:10.3390/atmos7080108, 2016.

616 Kuang, S., Newchurch, M. J., Burris, J., Wang, L., Buckley, P., Johnson, S., Knupp, K., Huang, G., Phillips, D., and
617 Cantrell, W.: Nocturnal ozone enhancement in the lower troposphere observed by lidar, *Atmos. Environ.*, 45, 6078-
618 6084, <https://doi.org/10.1016/j.atmosenv.2011.07.038>, 2011.

619 Kuang, S., Newchurch, M. J., Burris, J., and Liu, X.: Ground-based lidar for atmospheric boundary layer ozone
620 measurements, *Appl. Opt.*, 52, 3557-3566, <https://doi.org/10.1364/AO.52.003557>, 2013.

621 Kuang, S., Newchurch, M. J., Johnson, M. S., Wang, L., Burris, J., Pierce, R. B., Eloranta, E. W., Pollack, I. B., Graus,
622 M., de Gouw, J., Warneke, C., Ryerson, T. B., Markovic, M. Z., Holloway, J. S., Pour-Biazar, A., Huang, G., Liu,
623 X., and Feng, N.: Summertime tropospheric ozone enhancement associated with a cold front passage due to
624 stratosphere- to-troposphere transport and biomass burning: simultaneous ground-based lidar and airborne
625 measurements, *J. Geophys. Res.*, 122, 1293-1311, doi:10.1002/2016JD026078, 2017.

626 Kulawik, S. S., Bowman, K. W., Luo, M., Rodgers, C. D., and Jourdain, L.: Impact of nonlinearity on changing the a
627 priori of trace gas profile estimates from the Tropospheric Emission Spectrometer (TES), *Atmos. Chem. Phys.*, 8,
628 3081–3092, doi:10.5194/acp-8-3081-2008, 2008.

629 Leblanc, T., Sica, R. J., van Gijssel, J. A. E., Godin-Beekmann, S., Haeefe, A., Trickl, T., Payen, G., and Liberti, G.:
630 Proposed standardized definitions for vertical resolution and uncertainty in the NDACC lidar ozone and
631 temperature algorithms – Part 2: Ozone DIAL uncertainty budget, *Atmos. Meas. Tech.*, 9, 4051-4078,
632 10.5194/amt-9-4051-2016, 2016.

633 Langford, A. O., Alvarez, R. J., Brioude, J., Fine, R., Gustin, M. S., Lin, M. Y., Marchbanks, R. D., Pierce, R. B.,
634 Sandberg, S. P., Senff, C. J., Weickmann, A. M., and Williams, E. J.: Entrainment of stratospheric air and Asian
635 pollution by the convective boundary layer in the southwestern U.S., *J. Geophys. Res.*, 122, 1312-1337,
636 doi:10.1002/2016JD025987, 2017.

637 Lelieveld, J. and Dentener, F. J.: What controls tropospheric ozone?, *J. Geophys. Res.*, 105, 3531-3551,
638 doi:10.1029/1999JD901011, 2000.

639 Lin, M., Fiore, A. M., Horowitz, L. W., Langford, A. O., Oltmans, S. J., Tarasick, D., and Reider, H. E.: Climate
640 variability modulates western US ozone air quality in spring via deep stratospheric intrusions, *Nature*
641 *Communications*, 6, 7105, doi:10.1038/ncomms8105, 2015.

642 Lin, S. J. and Rood, R. B: Multidimensional flux form semi-Lagrangian transport schemes, *Mon. Weather Rev.*, 124,
643 2046-2070, [https://doi.org/10.1175/1520-0493\(1996\)124<2046:MFFSLT>2.0.CO;2](https://doi.org/10.1175/1520-0493(1996)124<2046:MFFSLT>2.0.CO;2), 1996.

644 Liu, X., Chance, K., Sioris, C. E., Spurr, R. J. D., Kurosu, T. P., Martin, R. V., and Newchurch, M. J.: Ozone profile
645 and tropospheric ozone retrievals from the Global Ozone Monitoring Experiment: Algorithm description and
646 validation, *J. Geophys. Res.-Atmos.*, 110, D20307, doi:10.1029/2005JD006240, 2005.

647 Liu, X., Bhartia, P. K., Chance, K., Spurr, R. J. D., and Kurosu, T. P.: Ozone profile retrievals from the Ozone
648 Monitoring Instrument, *Atmos. Chem. Phys.*, 10, 2521-2537, doi:10.5194/acp-10-2521-2010, 2010.

649 Lock, A. P., Brown, A. R., Bush, M. R., Martin, G. M., and Smith, R. N. B.: A new boundary layer mixing scheme.
650 Part I: Scheme description and single-column model tests, *Mon. Weather Rev.*, 128, 3187-3199,
651 [https://doi.org/10.1175/1520-0493\(2000\)128<3187:ANBLMS>2.0.CO;2](https://doi.org/10.1175/1520-0493(2000)128<3187:ANBLMS>2.0.CO;2), 2000.

652 Luo, M., Rinsland, C. P., Rodgers, C. D., Logan, J. A., Worden, H., Kulawik, S., Eldering, A., Goldman, A., Shephard,
653 M. W., Gunson, M., and Lampel, M.: Comparison of carbon monoxide measurements by TES and MOPITT:
654 influence of a priori data and instrument characteristics on nadir atmospheric species retrievals, *J. Geophys. Res.*,
655 112, D09303, doi:10.1029/2006JD007663, 2007.

656 Martin, R.: Satellite remote sensing of surface air quality, *Atmos. Environ.*, 42, 7823-7843
657 <http://dx.doi.org/10.1016/j.atmosenv.2008.07.018>, 2008.

658 Martin, R. V., Chance, K., Jacob, D. J., Kurosu, T. P., Spurr, R. J. D., Bucsel, E., Gleason, J. F., Palmer, P. I., Bey,
659 I., Fiore, A. M., Li, Q., Yantosca, R. M., and Koelemeijer, R. B. A.: An improved retrieval of tropospheric nitrogen
660 dioxide from GOME, *J. Geophys. Res.*, 107, 4437, <https://doi.org/10.1029/2001JD001027>, 2002.

661 McPeters, R. D., Labow, G. J., and Logan, J. A.: Ozone climatological profiles for satellite retrieval algorithms, *J.*
662 *Geophys. Res.*, 112, D05308, doi:10.1029/2005JD006823, 2007.

663 Molod, A., Takacs, L. L., Suarez, M. J., Bacmeister, J. T., Song, I.-S., and Eichmann, A.: The GEOS-5 Atmospheric
664 General Circulation Model: Mean Climate and Development from MERRA to Fortuna, *NASA Tech. Memo.*
665 104606, 28, Tech. Rep. Series on Global Modeling and Data Assimilation, edited by: Suarez, M. J., 117 pp., 2012.

666 Natraj, V., Liu, X., Kulawik, S., Chance, K., Chatfield, R., Edwards, D. P., Eldering, A., Francis, G., Kurosu, T.,
667 Pickering, K., Spurr, R., and Worden, H.: Multi-spectral sensitivity studies for the retrieval of tropospheric and
668 lowermost tropospheric ozone from simulated clear-sky GEO-CAPE measurements, *Atmos. Environ.*, 45, 7151-
669 7165, 2011.

670 Ott, L. E., Duncan, B. N., Thompson, A. M., Diskin, G., Fasnacht, Z., Langford, A. O., Lin, M., Molod, A. M., Nielsen,
671 J. E., Pusede, S. E.; et al.: Frequency and impact of summertime stratospheric intrusions over Maryland during
672 DISCOVER-AQ (2011): New evidence from NASA's GEOS-5 simulations, *J. Geophys. Res. Atmos.*, 121,
673 doi:10.1002/2015JD024052, 2016.

674 Putman, W. M. and Lin, S.-J.: Finite-volume transport on various cubed-sphere grids, *J. Comput. Phys.*, 227, 55-78,
675 doi:10.1016/j.jcp.2007.07.022, 2007.

676 Rienecker, M. M., Suarez, M. J., Todling, R., Bacmeister, J., Takacs, L., Liu, H.-C., Gu, W., Sienkiewicz, M., Koster,
677 R. D., Gelaro, R., Stajner, I., and Nielsen, J. E.: The GEOS-5 Data Assimilation System – Documentation of
678 Versions 5.0.1, 5.1.0, and 5.2.0, NASA/TM-2008-104606, 27, 101 pp, 2008.

679 Rodgers, C. D.: *Inverse Methods for Atmospheric Sounding*, World Scientific, River Edge, New Jersey, 2000.

680 Sauvage, B., Martin, R. V., van Donkelaar, A., Liu, X., Chance, K., Jaeglé, L., Palmer, P. I., Wu, S., and Fu, T.-M.:
681 Remote sensed and in situ constraints on processes affecting tropical tropospheric ozone, *Atmos. Chem. Phys.*, 7,
682 815-838, <https://doi.org/10.5194/acp-7-815-2007>, 2007.

683 Stohl, A., Bonasoni, P., Cristofanelli, P., Collins, W., Feichter, J., Frank, A., Forster, C., Gerasopoulos, E., Gaggeler,
684 H., James, P., Kentarchos, T., Kromp-Kolb, H., Kruger, B., Land, C., Meloen, J., Papayannis, A., Priller, A.,
685 Seibert, P., Sprenger, M., Roelofs, G. J., Scheel, H. E., Schnabel, C., Siegmund, P., Tobler, L., Trickl, T., Wernli,
686 H., Wirth, V., Zanis, P., and Zerefos, C.: Stratosphere-troposphere exchange: A review, and what we have learned
687 from STACCATO, *J. Geophys. Res.*, 108(D12), 8516, doi:10.1029/2002JD002490, 2003.

688 Sullivan, J. T., McGee, T. J., Thompson, A. M., Pierce, R. B., Sumnicht, G. K., Twigg, L. W., Eloranta, E., and Hoff,
689 R. M.: Characterizing the lifetime and occurrence of stratospheric-tropospheric exchange events in the rocky
690 mountain region using high-resolution ozone measurements, *J. Geophys. Res. Atmos.*, 120, 12410-12424,
691 doi:10.1002/2015JD023877, 2015a.

692 Sullivan, J. T., McGee, T. J., De Young, R., Sumnicht, G. K., Twigg, L. W., Pliutau, D., Carrion, W., and Knepp, T.:
693 Results from the NASA GSFC and LaRC ozone lidar intercomparison: New mobile tools for atmospheric research,
694 *J. Atmos. Ocean. Technol.*, 32, 1779-1795, 2015b.

695 Sullivan, J. T., McGee, T. J., Langford, A. O., Alvarez, R. J., Senff, C. J., Reddy, P. J., Thompson, A. M., Twigg, L.
696 W., Sumnicht, G. K., Lee, P., Weinheimer, A., Knote, C., Long, R. W., and Hoff, R. M.: Quantifying the
697 contribution of thermally driven recirculation to a high-ozone event along the Colorado Front Range using lidar,
698 *J. Geophys. Res.-Atmos.*, 121, 10377–10390, <https://doi.org/10.1002/2016JD025229>, 2016.

699 U.S. Environmental Protection Agency: *Air Quality Criteria for Ozone and Related Photochemical Oxidants (2006*
700 *Final)*, U.S. Environmental Protection Agency, Washington, DC, EPA/600/R-05/004aF-cF, 2006.

701 U.S. Environmental Protection Agency. *National Ambient Air Quality Standards for Ozone - Final Rule*, Federal
702 Register 80, 65292-65468, available at <https://www.gpo.gov/fdsys/pkg/FR-2015-10-26/pdf/2015-26594.pdf>,
703 2015.

704 Vu, K. T., Dingle, J. H., Bahreini, R., Reddy, P. J., Apel, E. C., Campos, T. L., DiGangi, J. P., Diskin, G. S., Fried,
705 A., Herndon, S. C., Hills, A. J., Hornbrook, R. S., Huey, G., Kaser, L., Montzka, D. D., Nowak, J. B., Pusede, S.
706 E., Richter, D., Roscioli, J. R., Sachse, G. W., Shertz, S., Stell, M., Tanner, D., Tyndall, G. S., Walega, J., Weibring,
707 P., Weinheimer, A. J., Pfister, G., and Flocke, F.: Impacts of the Denver Cyclone on regional air quality and aerosol
708 formation in the Colorado Front Range during FRAPPÉ 2014, *Atmos. Chem. Phys.*, 16, 12039-12058,
709 doi:10.5194/acp-16-12039-2016, 2016.

710 Wang, Y. H., Jacob, D. J., and Logan, J. A: Global simulation of tropospheric O₃-NO_x-hydrocarbon chemistry: 1.
711 Model formulation, *J. Geophys. Res.*, 103, 10713-10725, doi:10.1029/98JD00158, 1998.

712 Wargan, K., Pawson, S., Olsen, M. A., Witte, J. C., Douglass, A. R., Ziemke, J. R., Strahan, S. E., and Nielsen, J. E.:
713 The global structure of upper troposphere-lower stratosphere ozone in GEOS-5: A multiyear assimilation of EOS
714 Aura data, *J. Geophys. Res. Atmos.*, 120, 2013-2036, doi:10.1002/2014JD022493, 2015.

715 Worden, H. M., Logan, J. A., Worden, J. R., Beer, R., Bowman, K., Clough, S. A., Eldering, A., Fisher, B. M., Gunson,
716 M. R., Herman, R. L., Kulawik, S. S., Lampel, M. C., Luo, M., Megretskaia, I. A., Osterman, G. B., and Shephard,
717 M.W.: Comparisons of Tropospheric Emission Spectrometer (TES) ozone profiles to ozonesondes: Methods and
718 initial results, *J. Geophys. Res.*, 112, D03309, doi:10.1029/2006JD007258, 2007.

719 Wu, W.-S., Purser, R. J., and Parrish, D. F.: Three-dimensional variational analysis with spatially inhomogeneous
720 covariances, *Mon. Wea. Rev.*, 130, 2905-2916, [https://doi.org/10.1175/1520-](https://doi.org/10.1175/1520-0493(2002)130<2905:TDVAWS>2.0.CO;2)
721 [0493\(2002\)130<2905:TDVAWS>2.0.CO;2](https://doi.org/10.1175/1520-0493(2002)130<2905:TDVAWS>2.0.CO;2), 2002.

722 Zhang, L., Jacob, D. J., Liu, X., Logan, J. A., Chance, K., Eldering, A., and Bojkov, B. R.: Intercomparison methods
723 for satellite measurements of atmospheric composition: application to tropospheric ozone from TES and OMI,
724 *Atmos. Chem. Phys.*, 10, 4725-4739, <https://doi.org/10.5194/acp-10-4725-2010>, 2010.

725 Zoogman, P., Jacob, D. J., Chance, K., Liu, X., Lin, M., Fiore, A., and Travis, K.: Monitoring high-ozone events in
726 the US Intermountain West using TEMPO geostationary satellite observations, *Atmos. Chem. Phys.*, 14, 6261-
727 6271, <https://doi.org/10.5194/acp-14-6261-2014>, 2014.

728 Zoogman, P., Liu, X., Suleiman, R., Pennington, W., Flittner, D., Al-Saadi, J., Hilton, B., Nicks, D., Newchurch, M.,
729 Carr, J., Janz, S., Andraschko, M., Arola, A., Baker, B., Canova, B., Miller, C. C., Cohen, R., Davis, J., Dussault,
730 M., Edwards, D., Fishman, J., Ghulam, A., Abad, G. G., Grutter, M., Herman, J., Houck, J., Jacob, D., Joiner, J.,
731 Kerridge, B., Kim, J., Krotkov, N., Lamsal, L., Li, C., Lindfors, A., Martin, R., McElroy, C., McLinden, C., Natraj,
732 V., Neil, D., Nowlan, C., O'Sullivan, E., Palmer, P., Pierce, R., Pippin, M., Saiz-Lopez, A., Spurr, R., Szykman,
733 J., Torres, O., Veeffkind, J., Veihelmann, B., Wang, H., Wang, J., and Chance, K.: Tropospheric emissions:
734 Monitoring of pollution (TEMPO), *J. Quant. Spectrosc. Ra.*, 186, 17-39,
735 <https://doi.org/10.1016/j.jqsrt.2016.05.008>, 2017.

736 **Tables**737 **Table 1. Information about the TOLNet systems applied during this study.**

System Name	Latitude (°N)	Longitude (°W)	Elevation (m)^a	# of observations^b
TROPOZ	40.6	105.1	1569.0	21
JPL TMF	34.4	117.7	2285.0	26 ^c
RO3QET	34.7	86.6	206.0	12 ^d

738 ^aElevation of the topography above sea level.739 ^bNumber of days of lidar observations between July - August 2014.740 ^cJPL TMF lidar observations only taken during nighttime hours between July-August 2014.741 ^dRO3QET lidar observations only taken from the surface to ~5 km agl between July-August 2014.

742

743 **Table 2. Time-series evaluation of TB-Clim, GEOS-5 FP, MERRA2, and GEOS-Chem daily-averaged**
 744 **tropospheric and LMT column O₃ with the RO3QET, TROPOZ and JPL TMF lidars. The statistics include**
 745 **correlation (R), mean bias, bias standard deviation (1σ), and root mean squared error (RMSE).**

RO3QET	TB-Clim	GEOS-5 FP	MERRA2	GEOS-Chem
<i>Tropospheric Column O₃ (0-5 km)</i>				
Correlation (R)	-0.09	0.23	-0.10	0.61
Bias ± 1σ (ppb)	3.7 ± 6.0	2.8 ± 5.6	-0.7 ± 5.8	1.7 ± 4.2
RMSE (ppb)	6.81	6.14	5.61	4.34
<i>LMT Column O₃ (0-2 km)</i>				
Correlation (R)	-0.68	0.03	-0.19	0.83
Bias ± 1σ (ppb)	2.9 ± 9.7	-2.9 ± 8.5	-4.9 ± 8.0	-1.3 ± 4.4
RMSE (ppb)	9.75	8.65	9.06	4.39
TROPOZ	TB-Clim	GEOS-5 FP	MERRA2	GEOS-Chem
<i>Tropospheric Column O₃ (0-10 km)</i>				
Correlation (R)	-0.09	0.26	0.38	0.82
Bias ± 1σ (ppb)	2.2 ± 9.7	3.3 ± 10.0	-4.6 ± 9.1	2.4 ± 6.0
RMSE (ppb)	9.73	10.33	9.99	6.30
<i>LMT Column O₃ (0-2 km)</i>				
Correlation (R)	-0.15	-0.09	-0.18	0.47
Bias ± 1σ (ppb)	-11.1 ± 7.5	-4.4 ± 7.3	-7.4 ± 7.4	-6.7 ± 6.2
RMSE (ppb)	13.23	8.43	10.33	8.93
JPL TMF	TB-Clim	GEOS-5 FP	MERRA2	GEOS-Chem
<i>Tropospheric Column O₃ (0-10 km)</i>				
Correlation (R)	-0.35	0.76	0.80	0.72
Bias ± 1σ (ppb)	0.3 ± 18.7	-5.0 ± 13.8	-10.6 ± 13.4	-0.5 ± 14.6
RMSE (ppb)	18.38	14.41	16.86	14.29
<i>LMT Column O₃ (0-2 km)</i>				
Correlation (R)	-0.53	-0.21	0.22	0.49
Bias ± 1σ (ppb)	3.3 ± 13.6	-2.4 ± 12.7	-4.0 ± 11.7	0.9 ± 10.4
RMSE (ppb)	13.72	12.68	12.14	10.24

746

747

748 **Table 3. Time-series evaluation of the TB-Clim, GEOS-5 FP, MERRA2, and GEOS-Chem hourly-averaged**
 749 **tropospheric and LMT column O₃ with the RO3QET, TROPOZ and JPL TMF lidars. The statistics include**
 750 **correlation (R), mean bias, bias standard deviation (1σ), and root mean squared error (RMSE).**

RO3QET	TB-Clim	GEOS-5 FP	MERRA2	GEOS-Chem
<i>Tropospheric Column O₃ (0-5 km)</i>				
Correlation (R)	-0.54	-0.55	-0.51	0.68
Bias ± 1σ (ppb)	3.5 ± 1.4	2.6 ± 1.6	-1.2 ± 1.5	2.1 ± 1.1
RMSE (ppb)	3.77	2.98	1.86	2.37
<i>LMT Column O₃ (0-2 km)</i>				
Correlation (R)	0.20	0.55	-0.43	0.76
Bias ± 1σ (ppb)	1.9 ± 3.9	-3.3 ± 3.6	-5.9 ± 4.0	0.3 ± 2.6
RMSE (ppb)	4.20	4.73	7.04	2.45
TROPOZ	TB-Clim	GEOS-5 FP	MERRA2	GEOS-Chem
<i>Tropospheric Column O₃ (0-10 km)</i>				
Correlation (R)	-0.07	-0.38	-0.56	0.78
Bias ± 1σ (ppb)	2.6 ± 2.5	3.3 ± 2.6	-5.1 ± 3.2	2.2 ± 1.7
RMSE (ppb)	3.57	4.17	6.00	2.74
<i>LMT Column O₃ (0-2 km)</i>				
Correlation (R)	0.26	0.76	0.67	0.92
Bias ± 1σ (ppb)	-12.6 ± 6.9	-7.5 ± 6.6	-9.6 ± 6.9	-7.7 ± 4.8
RMSE (ppb)	14.25	9.91	11.70	9.01

751

752 **Table 4. Time-series evaluation of daily-averaged X_r predictions using the TB-Clim, GEOS-5 FP, MERRA2,**
753 **and GEOS-Chem data as a priori information in theoretical TEMPO retrievals of tropospheric and LMT**
754 **column O_3 values with RO3QET, TROPOZ and JPL TMF lidars. The statistics include correlation (R), mean**
755 **bias, bias standard deviation (1σ), root mean squared error (RMSE), and the number of occurrences where**
756 **error exceeds 10 ppb.**

RO3QET	TB-Clim	GEOS-5 FP	MERRA2	GEOS-Chem
<i>Tropospheric Column O_3 (0-5 km)</i>				
Correlation (R)	0.98	0.90	0.95	0.96
Bias $\pm 1\sigma$ (ppb)	1.4 ± 2.3	1.3 ± 2.7	-0.2 ± 2.5	1.0 ± 2.0
RMSE (ppb)	2.66	2.91	2.43	2.17
10 ppb error exceedance	0	0	0	0
<i>LMT Column O_3 (0-2 km)</i>				
Correlation (R)	0.52	0.65	0.73	0.94
Bias $\pm 1\sigma$ (ppb)	0.2 ± 6.1	-3.8 ± 5.5	-3.4 ± 5.1	-2.2 ± 2.5
RMSE (ppb)	5.88	6.44	5.97	3.26
10 ppb error exceedance	1	3	2	0
TROPOZ	TB-Clim	GEOS-5 FP	MERRA2	GEOS-Chem
<i>Tropospheric Column O_3 (0-10 km)</i>				
Correlation (R)	0.97	0.92	0.94	0.92
Bias $\pm 1\sigma$ (ppb)	-0.9 ± 4.2	-0.6 ± 4.8	-2.2 ± 4.4	-0.5 ± 2.7
RMSE (ppb)	4.21	4.72	4.85	2.66
10 ppb error exceedance	1	1	2	0
<i>LMT Column O_3 (0-2 km)</i>				
Correlation (R)	0.38	0.41	0.42	0.65
Bias $\pm 1\sigma$ (ppb)	-11.4 ± 6.2	-6.4 ± 6.3	-5.1 ± 5.9	-4.8 ± 4.8
RMSE (ppb)	12.95	8.85	7.67	6.71
10 ppb error exceedance	10	6	4	3
JPL TMF	TB-Clim	GEOS-5 FP	MERRA2	GEOS-Chem
<i>Tropospheric Column O_3 (0-10 km)</i>				
Correlation (R)	0.98	0.99	0.99	0.99
Bias $\pm 1\sigma$ (ppb)	-0.2 ± 4.0	-0.8 ± 3.1	-1.7 ± 3.0	-0.3 ± 3.3
RMSE (ppb)	3.97	3.14	3.42	3.29
10 ppb error exceedance	1	1	1	1
<i>LMT Column O_3 (0-2 km)</i>				
Correlation (R)	0.31	0.25	0.39	0.42
Bias $\pm 1\sigma$ (ppb)	3.1 ± 14.8	1.9 ± 13.7	4.8 ± 12.6	1.0 ± 12.7
RMSE (ppb)	14.87	13.57	13.27	12.54
10 ppb error exceedance	9	8	10	6

757

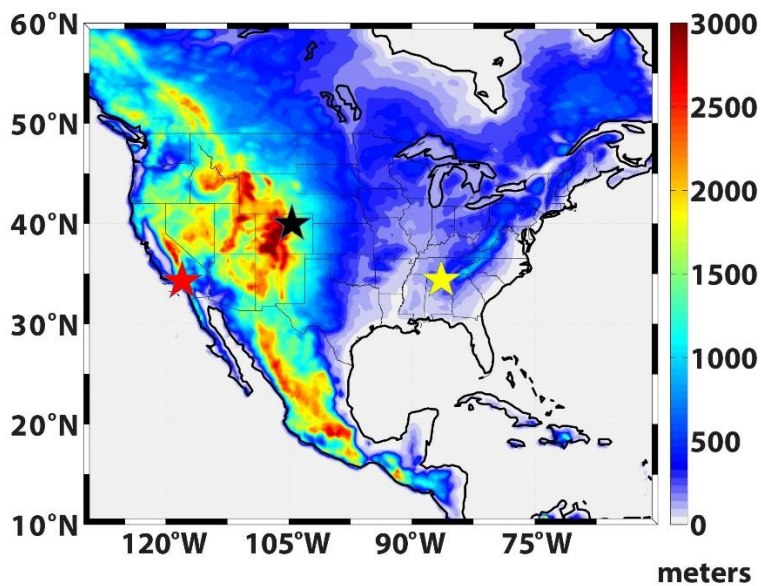
758

759 **Table 5. Time-series evaluation of hourly-averaged TOLNet observations and X_r predictions using the TB-**
 760 **Clim, GEOS-5 FP, MERRA2, and GEOS-Chem data as a priori information in theoretical TEMPO retrievals**
 761 **of tropospheric and LMT column O₃ values at the location of RO3QET (07 August, 2014) and TROPOZ (22**
 762 **July, 2014). The statistics include correlation (R), mean, min/max, and standard deviation (1σ) from**
 763 **observations and theoretical TEMPO retrievals.**

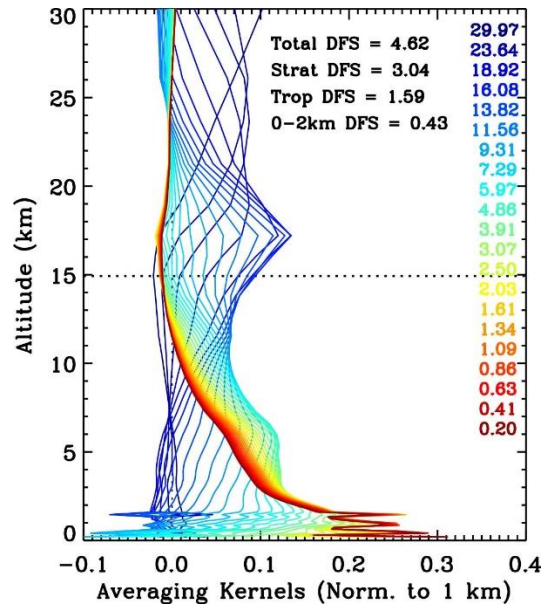
RO3QET 07 August, 2014	TOLNet*	TB-Clim	GEOS-5 FP	MERRA2	GEOS-Chem
<i>Tropospheric Column O₃ (0-5 km)</i>					
Correlation (R)	N/A	0.99	0.99	0.99	0.99
Mean (ppb)	60.7	59.8	59.5	59.0	59.5
Max/Min (ppb)	67.5/56.4	64.7/56.8	64.1/56.9	63.8/56.1	65.1/55.5
Std. Dev. (ppb)	3.62	2.63	2.35	2.55	3.18
<i>LMT Column O₃ (0-2 km)</i>					
Correlation (R)	N/A	0.98	0.98	0.99	0.98
Mean (ppb)	65.2	56.5	53.4	53.1	62.1
Max/Min (ppb)	79.4/54.3	62.6/52.5	59.4/49.8	59.4/48.8	70.6/54.6
Std. Dev. (ppb)	9.27	3.41	3.33	3.67	5.38
TROPOZ 22 July, 2014	TOLNet	TB-Clim	GEOS-5 FP	MERRA2	GEOS-Chem
<i>Tropospheric Column O₃ (0-10 km)</i>					
Correlation (R)	N/A	0.98	0.97	0.96	0.97
Mean (ppb)	50.5	52.4	52.2	50.7	50.3
Max/Min (ppb)	55.8/46.3	55.7/49.2	55.5/49.0	53.3/47.7	53.3/47.3
Std. Dev. (ppb)	3.25	2.60	2.52	2.06	2.40
<i>LMT Column O₃ (0-2 km)</i>					
Correlation (R)	N/A	0.85	0.51	0.79	0.98
Mean (ppb)	75.0	44.3	49.9	51.2	56.3
Max/Min (ppb)	97.0/58.6	47.5/41.3	54.3/45.6	54.9/47.3	66.4/47.8
Std. Dev. (ppb)	12.77	2.27	2.96	2.81	5.93

764 *Correlation values are computed between the O₃ climatology and models compared to observations (i.e., TOLNet)
 765 and therefore are presented as N/A for TOLNet.

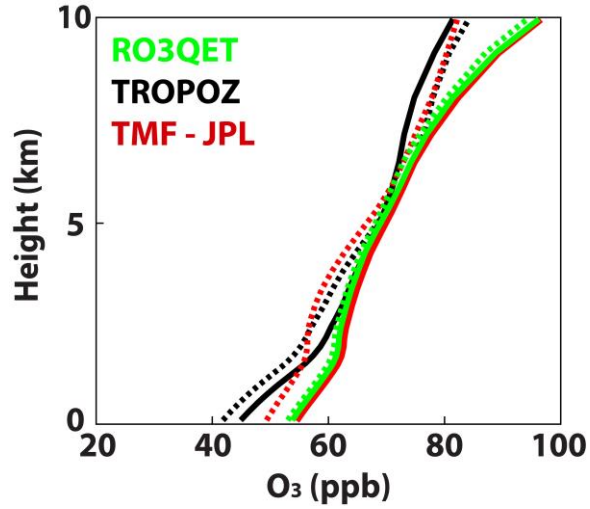
766



768
769 **Figure 1.** Location of the GSCF TROPOZ (black star), JPL TMF (red star), and the UAH RO3QET (yellow
770 star) TOLNet systems during the summer of 2014. The locations are overlaid on the topographic heights
771 (meters) from the GEOS-5 model.
772

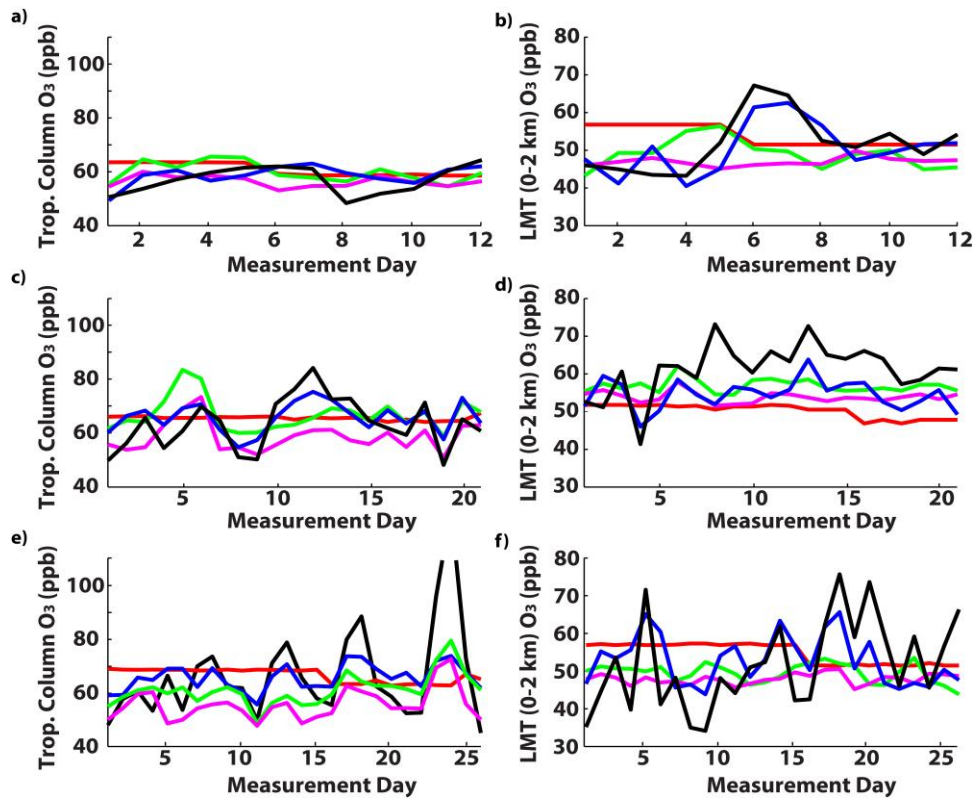


773
 774 Figure 2. Simulated TEMPO O₃ retrieval AK matrix (normalized to 1 km layer) from joint UV+VIS
 775 measurements (290-345 nm, 540-650 nm) from the surface to 30 km agl used at the UAH TOLNet site during
 776 August at 20 UTC. The AK lines are for individual vertical levels (km agl), with the colors ranging from red to
 777 blue representing vertical levels from surface air to ~30 km. The legend presents the DFS for the total (Total),
 778 stratosphere (Strat), troposphere (Trop), and 0-2 km columns.
 779



780

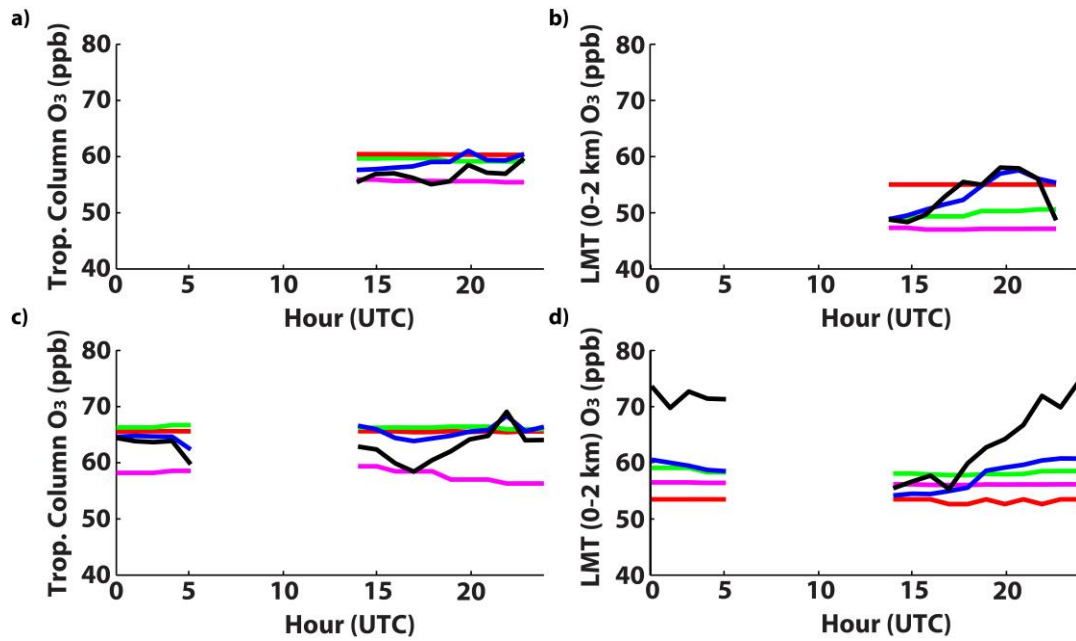
781 **Figure 3. Monthly-averaged vertical profiles of O₃ (ppb) from TB-Clim data at the location of the RO3QET**
 782 **(green lines), TROPOZ (black lines), and JPL TMF (red lines) TOLNet systems for July (solid lines) and August**
 783 **(dashed lines). The monthly-averages are derived using the hourly TB-Clim data during the hours/days of**
 784 **observations obtained at each location.**
 785



786

787 **Figure 4. Time-series of daily-averaged tropospheric column (0-10 km) O₃ (ppb) from TB-Clim (red line),**
 788 **GEOS-5 FP (green line), MERRA2 (magenta line), and GEOS-Chem (blue line) compared to TOLNet (black**
 789 **line) at the locations of a) RO3QET, c) TROPOZ, and e) JPL TMF. Panels b), d), and f) are similar but for the**
 790 **comparison of LMT column (0-2 km) O₃.**

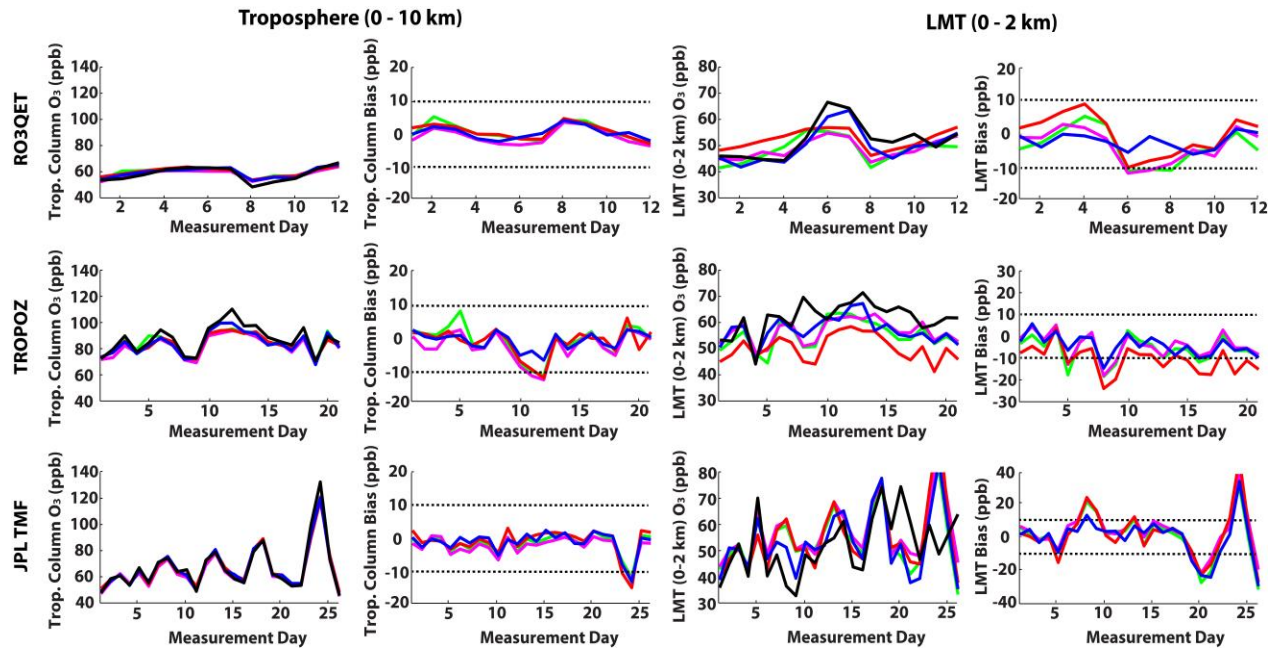
791



792

793 **Figure 5. Diurnal time-series of hourly-averaged tropospheric column (0-10 km) O₃ (ppb) from TB-Clim (red**
 794 **line), GEOS-5 FP (green line), MERRA2 (magenta line), and GEOS-Chem (blue line) compared to TOLNet**
 795 **(black line) at the locations of a) RO3QET and c) TROPOZ. Panels b) and d) are similar but for the comparison**
 796 **of LMT column (0-2 km) O₃. The times of missing data are hours where no TOLNet observations were taken**
 797 **during the summer of 2014.**

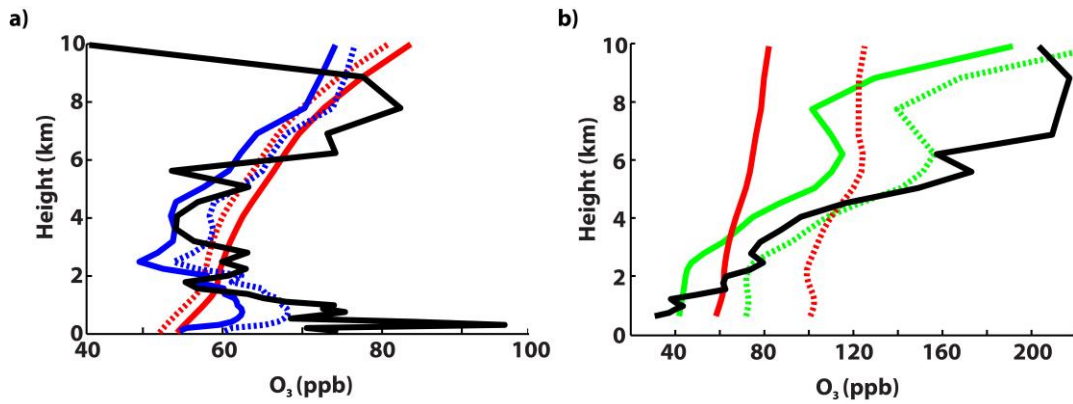
798



799

800 Figure 6. Time-series of daily-averaged tropospheric and LMT column X_r and bias values (ppb) when using
 801 TB-Clim (red line), GEOS-5 FP (green line), MERRA2 (magenta line), and GEOS-Chem (blue line) as the a
 802 priori when compared to observed O₃ by TOLNet (black line) at the locations of RO3QET (top row), TROPOZ
 803 (middle row), and JPL TMF (bottom row). The dashed black lines represent the 10 ppb precision/accuracy
 804 requirement for TEMPO O₃ retrievals.

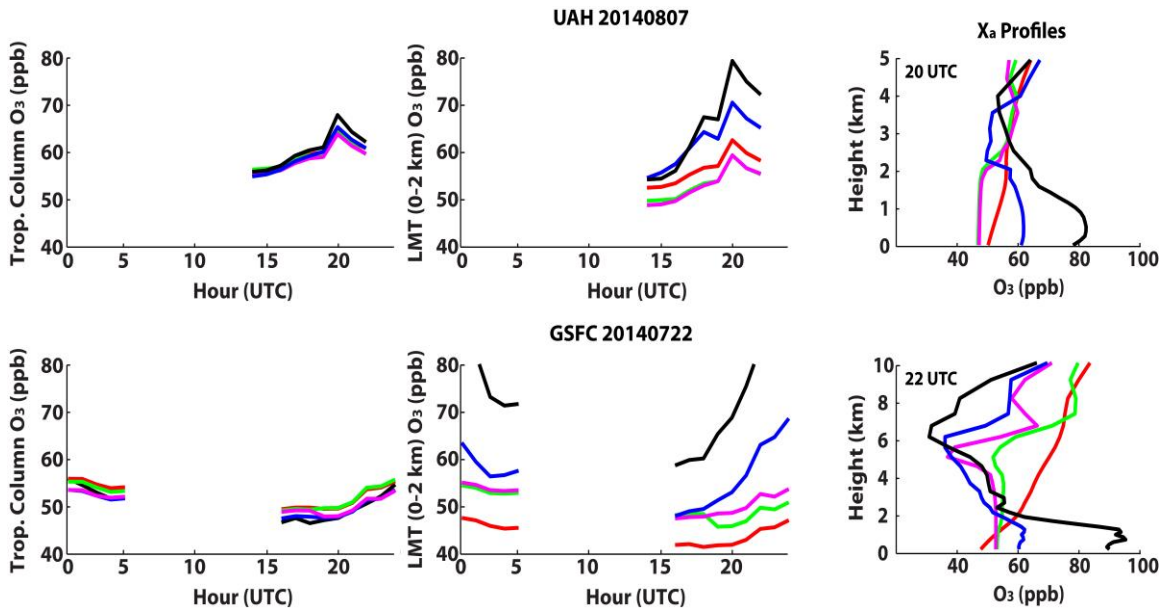
805



806

807 Figure 7. Vertical profiles of a) daily-averaged X_a (solid line) and X_r (dashed line) O_3 values when applying
 808 TB-Clim (red line) and GEOS-Chem (blue line) as a priori information in TEMPO retrievals compared to
 809 TOLNet (black line) at the locations of the JPL TMF lidar on 08 July, 2014. Panel b) shows daily-averaged X_a
 810 and X_r O_3 values when applying TB-Clim (red line) and GEOS-5 FP (green line) as a priori information in
 811 TEMPO retrievals compared to TOLNet (black line) at the locations of the JPL TMF lidar on 21 August, 2014.

812



813

814 **Figure 8.** Diurnal time-series of hourly-averaged tropospheric (0-10 km) and LMT (0-2 km) column X_r O₃
 815 (ppb) values with a priori from TB-Clim (red line), GEOS-5 FP (green line), MERRA2 (magenta line), and
 816 GEOS-Chem (blue line) compared to TOLNet (black line) at the locations of RO3QET location on 07 August
 817 2014 (top row) and TROPOZ on 22 July 2014 (bottom row). The hourly-averaged a priori vertical profiles are
 818 also presented (right column) along with TOLNet (black line) for the hour of largest LMT O₃ observed by
 819 TOLNet in the time-series.

820